

---

# Basic Principles of NMR

## 1.1. INTRODUCTION

Energy states and population distribution are the fundamental subjects of any spectroscopic technique. The energy difference between energy states gives rise to the frequency of the spectra, whereas intensities of the spectral peaks are proportional to the population difference of the states. Relaxation is another fundamental phenomenon in nuclear magnetic resonance spectroscopy (NMR), which influences both line shapes and intensities of NMR signals. It provides information about structure and dynamics of molecules. Hence, understanding these aspects lays the foundation to understanding basic principles of NMR spectroscopy.

In principle, an NMR spectrometer is more or less like a radio. In a radio, audio signals in the frequency range of kilohertz are the signals of interest, which one can hear. However, the signals sent by broadcast stations are in the range of 100 MHz for FM and of up to 1 GHz for AM broadcasting. The kilohertz audio signals must be separated from the megahertz transmission frequencies before they are sent to speakers. In NMR spectroscopy, nuclei have an intrinsic megahertz frequency which is known as the Larmor frequency. For instance, in a molecule, all protons have the same Larmor frequency. However, the signals of interest are the chemical shifts generated by the electron density surrounding an individual proton, which are in the kilohertz frequency range. Many of the protons in the molecule have different chemical environments which give different signals in the kilohertz range. One must find a way to eliminate the megahertz Larmor frequency in order to observe the kilohertz chemical shifts (more details to follow).

## 1.2. NUCLEAR SPIN IN A STATIC MAGNETIC FIELD

### 1.2.1. Precession of Nuclear Spins in a Magnetic Field

As mentioned above, energy and population associated with energy states are the basis of the frequency position and the intensity of spectral signals. In order to understand the principles of NMR spectroscopy, it is necessary to know how the energy states of nuclei are generated and what are the energy and population associated with the energy states.

Key questions to be addressed in this section include:

1. What causes nuclei to precess in the presence of a magnetic field?
2. What kind of nuclei will give NMR signals?
3. How do nuclear spins orient in the magnetic field?

Not any kind of nucleus will give NMR signals. Nuclei with an even number of both charge and mass have a spin quantum number of zero, for example,  $^{12}\text{C}$ . These kinds of nuclei do not have nuclear angular momentum and will not give rise to an NMR signal; these are called NMR inactive nuclei. For nuclei with a nonzero spin quantum number, energy states are produced by the nuclear angular momentum interacting with the applied magnetic field. Nuclei with a nonzero spin quantum number possess nuclear angular momentum whose magnitude is determined by:

$$P = \hbar\sqrt{I(I+1)} \quad (1.1)$$

in which  $I$  is the nuclear spin quantum number and  $\hbar$  is the Planck constant divided by  $2\pi$ . The value of  $I$  is dependent on the mass and charge of the nucleus and can be either an integral or half integral number. The  $z$  component of the angular momentum  $P_z$  is given by:

$$P_z = \hbar m \quad (1.2)$$

in which the magnetic quantum number  $m$  has possible values of  $I, I-1, \dots, -I+1, -I$ , and a total of  $2I+1$ . This equation tells us that the projection of nuclear angular momentum on the  $z$  axis is quantized in space and has a total of  $2I+1$  possible values. The orientations of nuclear angular momentum are defined by the allowed  $m$  values. For example, for spin  $\frac{1}{2}$  nuclei, the allowed  $m$  are  $\frac{1}{2}$  and  $-\frac{1}{2}$ . Thus, the angular momentum of spin  $\frac{1}{2}$  has two orientations; one is pointing up (pointing to the  $z$  axis) and the other pointing down (pointing to the  $-z$  axis) with an angle of  $54.7^\circ$  relative to the magnetic field (Figure 1.1).

The nuclei with a nonzero spin quantum number will rotate about the magnetic field  $B_0$  due to the torque generated by the interaction of the nuclear angular momentum with the magnetic field. The magnetic moment (or nuclear moment),  $\mu$ , is either parallel or antiparallel to their angular momentum:

$$\mu = \gamma P = \gamma \hbar\sqrt{I(I+1)} \quad (1.3)$$

in which  $\gamma$  is the nuclear gyromagnetic ratio, which has a specific value for a given isotope. Thus,  $\gamma$  is a characteristic constant for a specific nucleus. The angular momentum  $P$  is the same for all nuclei with the same magnetic quantum number, whereas the angular moment  $\mu$

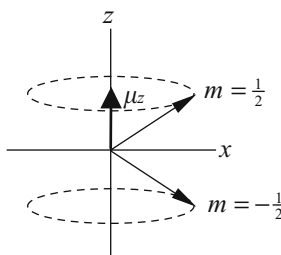


**Figure 1.1.** Orientation of nuclear angular momentum  $\mu$  with spin  $\frac{1}{2}$  and its  $z$  component,  $\mu_z$ . The vectors represent the angular momentum  $\mu$  rotating about the magnetic field whose direction is along the  $z$  axis of the laboratory frame.

is different for different nuclei. For instance,  $^{13}\text{C}$  and  $^1\text{H}$  have the same angular momentum  $P$  because they have same spin quantum number of  $\frac{1}{2}$ , but have different angular moments  $\mu$  because they are different isotopes with different  $\gamma$ . Therefore, the nuclear angular momentum  $\mu$  is used to characterize nuclear spins. The moment  $\mu$  is parallel to the angular momentum if  $\gamma$  is positive or antiparallel if  $\gamma$  is negative (e.g.,  $^{15}\text{N}$ ). Similar to the  $z$  component of the angular momentum,  $P_z$ , the  $z$  component of angular momentum  $\mu_z$  is given by:

$$\mu_z = \gamma P_z = \gamma \hbar m \quad (1.4)$$

The equation indicates that  $\mu_z$  has a different value for different nuclei even if they may have the same magnetic quantum number  $m$ . When nuclei with a nonzero spin quantum number are placed in a magnetic field, they will precess about the magnetic field due to the torque generated by the interaction of the magnetic field  $B_0$  with the nuclear moment  $\mu$ . The angle of  $\mu$  relative to  $B_0$  is dependent on  $m$ . Nuclei with nonzero spin quantum numbers are also called nuclear spins because their angular moments make them spin in the magnetic field.

In summary, the nuclear angular momentum is what causes the nucleus to rotate relative to the magnetic field. Different nuclei have a characteristic nuclear moment because the moment is dependent on the gyromagnetic ratio  $\gamma$ , whereas nuclei with the same spin quantum number possess the same nuclear angular momentum. Nuclear moments have quantized orientations defined by the value of the magnetic quantum number,  $m$ . The interaction of nuclei with the magnetic field is utilized to generate an NMR signal. Because the energy and population of nuclei are proportional to the magnetic field strength (more details discussed below), the frequency and intensity of the NMR spectral signals are dependent on the field strength.

### 1.2.2. Energy States and Population

It has been illustrated in the previous section that nuclei with nonzero spin quantum numbers orient along specific directions with respect to the magnetic field. They are rotating continuously about the field direction due to the nuclear moment  $\mu$  possessed by nuclei. For each orientation state, also known as the Zeeman state or spin state, there is energy associated with it, which is characterized by the frequency of the precession.

Key questions to be addressed in this section include:

1. What is the energy and population distribution of the Zeeman states?
2. What are the nuclear precession frequencies of the Zeeman states and the frequency of the transition between the states, and how are they different?
3. How are energy and population related to measurable spectral quantities?

The intrinsic frequency of the precession is the Larmor frequency  $\omega_0$ . The energy of the Zeeman state with magnetic quantum number  $m$  can be described in terms of the Larmor frequency:

$$E = -\mu_z B_0 = -m \hbar \gamma B_0 = m \hbar \omega_0 \quad (1.5)$$

in which  $B_0$  is the magnetic field strength in the unit of tesla, T, and  $\omega_0 = -\gamma B_0$  is the Larmor frequency. Therefore, the energy difference of the allowed transition (the selection rule is that

only a single-quantum transition, that is,  $\Delta m = \pm 1$ , is allowed), for instance, between the  $m = -\frac{1}{2}$  and  $m = \frac{1}{2}$  Zeeman states, is given by:

$$\Delta E = \hbar \gamma B_0 \quad (1.6)$$

Because  $\Delta E = \hbar \omega$ , the frequency of the required electromagnetic radiation for the transition has the form of:

$$\omega = \gamma B_0 \quad (1.7)$$

which has a linear dependence on the magnetic field strength. Commonly, the magnetic field strength is described by the proton Larmor frequency at the specific field strength. A proton resonance frequency of 100 MHz corresponds to the field strength of 2.35 T. For example, a 600 MHz magnet has a field strength of 14.1 T. While the angular frequency  $\omega$  has a unit of radians per second, the frequency can also be represented in hertz with the relationship of:

$$\nu = \frac{\omega}{2\pi} \quad (1.8)$$

As the magnetic field strength increases, the energy difference between two transition states becomes larger, as does the frequency associated with the Zeeman transition. The intensity of the NMR signal comes from the population difference between two Zeeman states of the transition. The population of the energy state is governed by the Boltzmann distribution. For a spin  $\frac{1}{2}$  nucleus with a positive  $\gamma$  such as  $^1\text{H}$ , or  $^{13}\text{C}$ , the lower energy state (ground state) is defined as the  $\alpha$  state for  $m = \frac{1}{2}$ , whereas the higher energy state (excited state) is labeled as the  $\beta$  state for  $m = -\frac{1}{2}$ . For  $^{15}\text{N}$ ,  $m = -\frac{1}{2}$  is the lower energy  $\alpha$  state because of its negative  $\gamma$ . The ratio of the populations in the states is quantitatively described by the Boltzmann equation:

$$\frac{N_\beta}{N_\alpha} = e^{-\Delta E/kT} = e^{-\hbar \gamma B_0/kT} = \frac{1}{e^{\hbar \gamma B_0/kT}} \quad (1.9)$$

in which  $N_\alpha$  and  $N_\beta$  are the population of the  $\alpha$  and  $\beta$  states, respectively,  $T$  is the absolute temperature and  $k$  is the Boltzmann constant. The equation states that both the energy difference of the transition states and the population difference of the states increase with the magnetic field strength. Furthermore, the population difference has a temperature dependence. If the sample temperature reaches absolute zero, there is no population at the  $\beta$  state and all spins will lie in the  $\alpha$  state, whereas both states will have equal population if the temperature is infinitely high. At  $T$  near room temperature,  $\sim 300$  K,  $\hbar \gamma B_0 \ll kT$ . As a consequence, a first-order Taylor expansion can be used to describe the population difference:

$$\frac{N_\beta}{N_\alpha} \approx 1 - \frac{\hbar \gamma B_0}{kT} \quad (1.10)$$

At room temperature, the population of the  $\beta$  state is slightly lower than that of the  $\alpha$  state. For instance, the population ratio for protons at 800 MHz field strength is 0.99987. This indicates that only a small fraction of the spins will contribute to the signal intensity due to the low energy difference and hence NMR spectroscopy intrinsically is a very insensitive

spectroscopic technique. Therefore, a stronger magnetic field is necessary to obtain better sensitivity, in addition to other advantages such as higher resolution and the TROSY effect (transverse relaxation optimized spectroscopy).

### 1.2.3. Bulk Magnetization

Questions to be addressed in this section include:

1. What is the bulk magnetization and where is it located?
2. Why do no transverse components of bulk magnetization exist at equilibrium?

The observable NMR signals come from the assembly of nuclear spins in the presence of the magnetic field. It is the bulk magnetization of a sample (or macroscopic magnetization) that gives the observable magnetization, which is the vector sum of all spin moments (nuclear angular moments). Because nuclear spins precess about the magnetic field along the  $z$  axis of the laboratory frame, an individual nuclear moment has equal probability of being in any direction of the  $xy$  plane. Accordingly, the transverse component of the bulk magnetization at the equilibrium state is averaged to zero and hence is not observable (Figure 1.2). The bulk magnetization  $M_0$  results from the small population difference between the  $\alpha$  and  $\beta$  states. At equilibrium, this vector lies along the  $z$  axis and is parallel to the magnetic field direction for nuclei with positive  $\gamma$  because the spin population in the  $\alpha$  state is larger than that in the  $\beta$  state. Although the bulk magnetization is stationary along the  $z$  axis, the individual spin moments rotate about the axis.

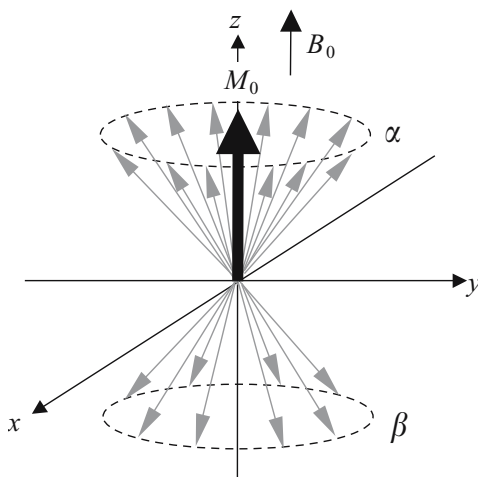


**Figure 1.2.** Bulk magnetization of spin  $\frac{1}{2}$  nuclei with positive  $\gamma$ .  $x$ ,  $y$ , and  $z$  are the axes of the laboratory frame. The thin arrows represent individual nuclear moments. The vector sum of the nuclear moments on the  $xy$  plane is zero because an individual nuclear moment has equal probability of being in any direction of the  $xy$  plane. The bulk magnetization  $M_0$ , labeled as a thick arrow, is generated by the small population difference between the  $\alpha$  and  $\beta$  states, and is parallel to the direction of the static magnetic field  $B_0$ .

### 1.3. ROTATING FRAME

The questions to be addressed in this section include:

1. What is the rotating frame and why is it needed?
2. What is the  $B_1$  field and why must it be an oscillating electromagnetic field?
3. How does the bulk magnetization  $M_0$  react when a  $B_1$  field is applied to it?
4. What is the relationship between radio frequency (RF) pulse power and pulse length?

The Larmor frequency of a nuclear isotope is the resonance frequency of the isotope in the magnetic field. For example,  $^1\text{H}$  Larmor frequency will be 500 MHz for all protons of a sample in a magnetic field of 11.75 T. If the Larmor frequency were the only observed NMR signal, NMR spectroscopy would not be useful because there would be only one resonance signal for all  $^1\text{H}$ . In fact, chemical shifts are the NMR signals of interest (details in section 1.7), which have a frequency range of kilohertz, whereas the Larmor frequency of all nuclei is in the range of megahertz. For instance, the observed signals of protons are normally in the range of several kilohertz with a Larmor frequency of 600 MHz in a magnetic field of 14.1 T. How the Larmor frequency is removed before NMR data are acquired, what the rotating frame is, why we need it, and how the bulk magnetization changes upon applying an additional electromagnetic field are the topics of this section.

Since the Larmor frequency will not be present in any NMR spectrum, it is necessary to remove its effect when dealing with signals in the kilohertz frequency range. This can be done by applying an electromagnetic field  $B_1$  on the  $xy$  plane of the laboratory frame, which rotates at the Larmor frequency with respect to the  $z$  axis of the laboratory frame. This magnetic field is used for the purposes of (a) removing the effect of the Larmor frequency and hence simplifying the theoretical and practical consideration of the spin precession in NMR experiments and (b) inducing the nuclear transition between two energy states by its interaction with the nuclei in the sample according to the resonance condition that the transition occurs when the frequency of the field equals the resonance frequency of the nuclei. This magnetic field is turned on only when it is needed. Because the Larmor frequency is not observed in NMR experiments, a new coordinate frame is introduced to eliminate the Larmor frequency from consideration, called the rotating frame. In the rotating frame, the  $xy$  plane of the laboratory frame is rotating at or near the Larmor frequency  $\omega_0$  with respect to the  $z$  axis of the laboratory frame. The transformation of the laboratory frame to the rotating frame can be illustrated by taking a merry-go-round as an example. The merry-go-round observed by one standing on the ground is rotating at a given speed. When one is riding on it, he is also rotating at the same speed. However, he is stationary relative to others on the merry-go-round. If the ground is considered as the laboratory frame, the merry-go-round is the rotating frame. When the person on the ground steps onto the merry-go-round, it is transformed from the laboratory frame to the rotating frame. The sole difference between the laboratory frame and the rotating frame is that the rotating frame is rotating in the  $xy$  plane about the  $z$  axis relative to the laboratory frame.

By transforming from the laboratory frame to the rotating frame, the nuclear moments are no longer spinning about the  $z$  axis, that is, they are stationary in the rotating frame. The term “transforming” here means that everything in the laboratory frame will rotate at a frequency of  $-\omega_0$  about the  $z$  axis in the rotating frame. As a result, the bulk magnetization does not have its Larmor frequency in the rotating frame. Since the applied  $B_1$  field is rotating at the Larmor frequency in the laboratory frame, the transformation of this magnetic field to the rotating frame results in a stationary  $B_1$  field along an axis on the  $xy$  plane in the rotating frame, for

example the  $x$  axis. Therefore, when this  $B_1$  magnetic field is applied, its net effect on the bulk magnetization is to rotate the bulk magnetization away from the  $z$  axis clockwise about the axis of the applied field by the left-hand rule in the vector representation.

In practice, the rotation of the  $B_1$  field with respect to the  $z$  axis of the laboratory frame is achieved by generating a linear oscillating electromagnetic field with the magnitude of  $2B_1$  because it is easily produced by applying electric current through the probe coil (Figure 1.3). The oscillating magnetic field has a frequency equal to or near the Larmor frequency of the nuclei. As the current increases from zero to maximum, the field proportionally increases from zero to the maximum field along the coil axis ( $2B_1$  in Figure 1.3). Reducing the current from the maximum to zero and then to the minimum (negative maximum,  $-i$ ) decreases the field from  $2B_1$  to  $-2B_1$ . Finally, the field is back to zero from  $-2B_1$  as the current is increased from the minimum to zero to finish one cycle. If the frequency of changing the current is  $\nu_{\text{rf}}$ , we can describe the oscillating frequency as  $\omega_{\text{rf}} (\omega = 2\pi\nu)$ . Mathematically, this linear oscillating field (thick arrow in Figure 1.4) can be represented by two equal fields with half of the magnitude,  $B_1$ , rotating in the  $xy$  plane at the same angular frequency in opposite directions to each other (thin arrows). When the field has the maximum strength at  $2B_1$ , each component aligns on the  $y$  axis with a magnitude of  $B_1$ . The vector sum of the two is  $2B_1$  [Figure 1.4(a)]. When the current is zero, which gives zero in the field magnitude, each component still has the same magnitude of  $B_1$  but aligns on the  $x$  and  $-x$  axes, respectively, which gives rise to a vector sum of zero [Figure 1.4(c)]. As the current reduces, both components rotate into

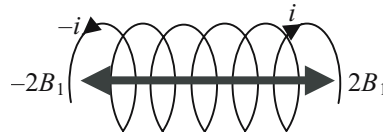


**Figure 1.3.** The electromagnetic field generated by the current passing through the probe coil. The magnitude of the field is modulated by changing the current between  $-i$  and  $+i$ . The electromagnetic field is called the oscillating  $B_1$  field.

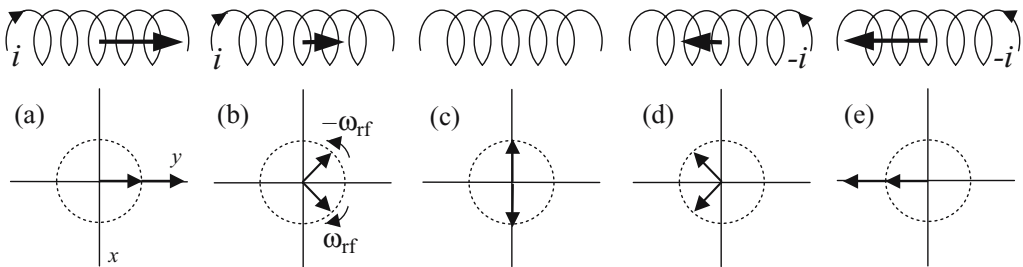


**Figure 1.4.** Vector sum of the oscillating  $B_1$  field generated by passing current through a probe coil. The magnitude of the field can be represented by two equal amplitude vectors rotating in opposite directions. The angular frequency of the two vectors is the same as the oscillating frequency  $\omega_{\text{rf}}$  of the  $B_1$  field. When  $\omega_{\text{rf}} = \omega_0$ ,  $B_1$  is said to be on resonance. (a) When the current reaches the maximum, the two vectors align on  $y$  axis. The sum of the two vectors is the same as the field produced in the coil. (b) As the  $B_1$  field reduces, its magnitude equals the sum of the projections of two vectors on the  $y$  axis. (c) When the two vectors are oppositely aligned on the  $x$  axis, the current in the coil is zero.

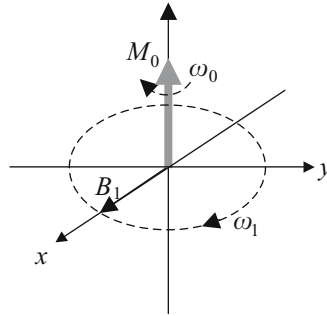


**Figure 1.5.**  $B_1$  field in the laboratory frame. The bulk magnetization  $M_0$  is the vector sum of individual nuclear moments which are precessing about the static magnetic field  $B_0$  at the Larmor frequency  $\omega_0$ . When the angular frequency  $\omega_{rf}$  of the  $B_1$  field is equal to the Larmor frequency, that is,  $\omega_{rf} = \omega_0$ , the  $B_1$  field is on resonance.

the  $-y$  region and the sum produces a negative magnitude [Figure 1.4(d)]. Finally, the two components meet at the  $-y$  axis, which represents a field magnitude of  $-2B_1$  [Figure 1.4(e)]. At any given time the two decomposed components have the same magnitude of  $B_1$ , the same frequency of  $\omega_{rf}$ , and are mirror images of each other.

If the frequency of the rotating frame is set to  $\omega_{rf}$ , which is close to the Larmor frequency  $\omega_0$ , the component of the  $B_1$  field which has  $\omega_1$  in the laboratory frame has null frequency in the rotating frame because of the transformation by  $-\omega_{rf}$ . The other with  $-\omega_{rf}$  in the laboratory frame now has an angular frequency of  $-2\omega_{rf}$  after the transformation. Since the latter has a frequency far away from the Larmor frequency it will not interfere with the NMR signals which are in the range of kilohertz. Therefore, this component will be ignored throughout the discussion unless specifically mentioned. The former component with null frequency in the rotating frame is used to represent the  $B_1$  field. If we regulate the frequency of the current oscillating into the coil as  $\omega_0$ , then setting  $\omega_{rf}$  equal to the Larmor frequency  $\omega_0$ , the  $B_1$  field is said to be on resonance (Figure 1.5). Since in the rotating frame the Larmor frequency is not present in the nuclei, the effect of  $B_0$  on nuclear spins is eliminated. The only field under consideration is the  $B_1$  field. From the earlier discussion we know that nuclear magnetization will rotate about the applied field direction upon its interaction with a magnetic field. Hence, whenever  $B_1$  is turned on, the bulk magnetization will be rotated about the axis where  $B_1$  is applied in the rotating frame. The frequency of the rotation is determined by:

$$\omega_1 = -\gamma B_1 \quad (1.11)$$

This should not be misunderstood as  $\omega_{rf}$  of the  $B_1$  field since  $\omega_{rf}$  is the field oscillating frequency determined by changing the direction of the current passing through the coil, which is set to be the same as or near the Larmor frequency. Frequency  $\omega_{rf}$  is often called the carrier frequency or the transmitter frequency. The frequency  $\omega_1$  is determined by the amplitude of the  $B_1$  field, that is, the maximum strength of the  $B_1$  field. By modulating the amplitude and time during which  $B_1$  is turned on, the bulk magnetization can be rotated to anywhere in the plane perpendicular to the axis of the applied  $B_1$  field in the rotating frame. If  $B_1$  is turned on and then turned off when  $M_0$  moves from the  $z$  axis to the  $xy$  plane, this is called a  $90^\circ$  pulse.



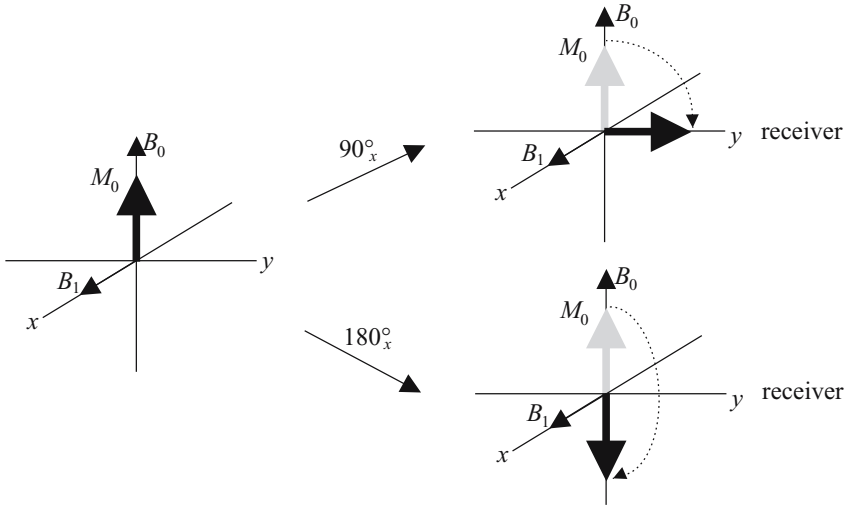


**Figure 1.6.** Vector representation of the bulk magnetization upon applying a  $90^\circ$  pulse and a  $180^\circ$  pulse by  $B_1$  along the  $x$  axis in the rotating frame.

The corresponding time during which  $B_1$  is applied is called the  $90^\circ$  pulse length (or the  $90^\circ$  pulse width), and the field amplitude is called the pulse power. A  $90^\circ$  pulse length can be as short as a few microseconds and as long as a fraction of a second. The pulse power for a hard (short)  $90^\circ$  pulse is usually as high as half of a hundred watts for protons and several hundred watts for heteronuclei (all nuclei except  $^1\text{H}$ ). Because heteronuclei have lower gyromagnetic ratios than protons, they have longer  $90^\circ$  pulse lengths at a given  $B_1$  field strength.

The  $90^\circ$  pulse length ( $\text{pw}_{90}$ ) is proportional to the  $B_1$  field strength:

$$\nu_1 = \frac{\gamma B_1}{2\pi} = \frac{1}{4\text{pw}_{90}} \quad (1.12)$$

$$\text{pw}_{90} = \frac{\pi}{2\gamma B_1} = \frac{1}{4\nu_1} \quad (1.13)$$

in which  $\nu_1$  is the field strength in the frequency unit of hertz. A higher  $B_1$  field produces a shorter  $90^\circ$  pulse. A  $90^\circ$  pulse of  $10 \mu\text{s}$  corresponds to a 25 kHz  $B_1$  field. Nuclei with smaller gyromagnetic ratios will require a higher  $B_1$  to generate the same  $\text{pw}_{90}$  as that with larger  $\gamma$ . When a receiver is placed on the transverse plane of the rotating frame, NMR signals are observed from the transverse magnetization. The maximum signal is obtained when the bulk magnetization is in the  $xy$  plane of the rotating frame, which is done by applying a  $90^\circ$  pulse. No signal is observed when a  $180^\circ$  pulse is applied (Figure 1.6).

#### 1.4. BLOCH EQUATIONS

As we now know, the nuclei inside the magnet produce nuclear moments which cause them to spin about the magnetic field. In addition, the interaction of the nuclei with the magnetic

field will rotate the magnetization toward the transverse plane when the electromagnetic  $B_1$  field is applied along a transverse axis in the rotating frame. After the pulse is turned off, the magnetization is solely under the effect of the  $B_0$  field. How the magnetization changes with time can be described by the Bloch equations, which are based on a simple vector model.

Questions to be addressed in the current section include:

1. What phenomena do the Bloch equations describe?
2. What is free induction decay (FID)?
3. What are the limitations of the Bloch equations?

In the presence of the magnetic field  $B_0$ , the torque produced by  $B_0$  on spins with the angular momentum  $\mu$  causes precession of the nuclear spins. Felix Bloch derived simple semi-classical equations to describe the time-dependent phenomena of nuclear spins in the static magnetic field (Bloch, 1946). The torque on the bulk magnetization, described by the change of the angular momentum as a function of time, is given by:

$$T = \frac{dP}{dt} = M \times B \quad (1.14)$$

in which  $M \times B$  is the vector product of the bulk magnetization  $M$  (the sum of  $\mu$ ) with the magnetic field  $B$ . Because  $M = \gamma P$  (or  $P = M/\gamma$ ) according to Equation (1.3), the change of magnetization with time is described by:

$$\frac{dM}{dt} = \gamma(M \times B) \quad (1.15)$$

When  $B$  is the static magnetic field  $B_0$  which is along the  $z$  axis of the laboratory frame, the change of magnetization along the  $x$ ,  $y$ , and  $z$  axes with time can be obtained from the determinant of the vector product:

$$\frac{dM}{dt} = i \frac{dM_x}{dt} + j \frac{dM_y}{dt} + k \frac{dM_z}{dt} = \gamma \begin{vmatrix} i & j & k \\ M_x & M_y & M_z \\ 0 & 0 & B_0 \end{vmatrix} = i\gamma M_y B_0 - j\gamma M_x B_0 \quad (1.16)$$

in which  $i$ ,  $j$ ,  $k$  are the unit vectors along the  $x$ ,  $y$ , and  $z$  axes, respectively. Therefore,

$$\frac{dM_x}{dt} = \gamma M_y B_0 \quad (1.17)$$

$$\frac{dM_y}{dt} = -\gamma M_x B_0 \quad (1.18)$$

$$\frac{dM_z}{dt} = 0 \quad (1.19)$$

The above Bloch equations describe the time dependence of the magnetization components under the effect of the static magnetic field  $B_0$  produced by the magnet of an NMR spectrometer without considering any relaxation effects. The  $z$  component of the bulk magnetization  $M_z$  is independent of time, whereas the  $x$  and  $y$  components are decaying as a function of time and the rate of decay is dependent on the field strength and nuclear gyromagnetic ratio. The

Bloch equations can be represented in the rotating frame, which is related to their form in the laboratory frame according to the following relationship:

$$\left(\frac{dM}{dt}\right)_{\text{rot}} = \left(\frac{dM}{dt}\right)_{\text{lab}} + M \times \omega = M \times (\gamma B + \omega) = M \times \gamma B_{\text{eff}} \quad (1.20)$$

in which  $B_{\text{eff}} = B + \omega/\gamma$  and  $\omega$  is the angular frequency of the rotating frame and is the same as  $\omega_{\text{rf}}$ . The motion of magnetization in the rotating frame is the same as in the laboratory frame, provided the field  $B$  is replaced by the effective field  $B_{\text{eff}}$ . When  $\omega = -\gamma B = \omega_0$ , the effective field disappears, resulting in time-independent magnetization in the rotating frame. It is worth noting that  $-\gamma B$  is the Larmor frequency of the magnetization according to Equation (1.5), whereas  $\gamma B$  is the transformation from the laboratory frame to the rotating frame,  $-\omega_{\text{rf}}$  (section 1.3).

Since the bulk magnetization at equilibrium is independent of time, based on the Bloch equations it is not an observable NMR signal. The observable NMR signals are the time-dependent transverse magnetization. However, at equilibrium the net  $xy$  projections of the magnetization (nuclear angular moments) are zero due to precession of the nuclear spins. The simple solution to this is to bring the bulk magnetization to the  $xy$  plane by applying the  $B_1$  electromagnetic field. The transverse magnetization generated by the  $B_1$  field ( $90^\circ$  pulse) will not stay in the transverse plane indefinitely, instead it decays under the interaction of the static magnetic field  $B_0$  while precessing about the  $z$  axis and realigns along the magnetic field direction or the  $z$  axis of the laboratory frame (Figure 1.7). The decay of the transverse magnetization forms the observable NMR signals detected by the receiver in the  $xy$  plane in the rotating frame, which is called the free induction decay, or FID.

The Bloch theory has its limitations in describing spin systems with nuclear interactions other than chemical shift interactions, such as strong scalar coupling. In general, the Bloch equations are applied to systems of noninteracting spin  $\frac{1}{2}$  nuclei. Nevertheless, it remains a very useful tool to illustrate simple NMR experiments.

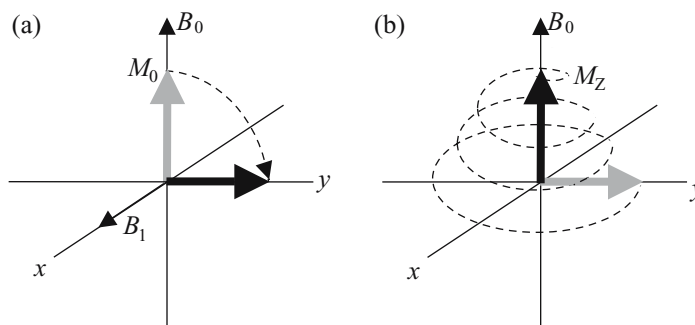


**Figure 1.7.** Vector model representation of a one-pulse experiment. (a) The equilibrium bulk magnetization shown by the shaded arrow is brought to the  $y$  axis by a  $90^\circ$  pulse along the  $x$  axis. (b) After the  $90^\circ$  pulse, the transverse magnetization decays back to the initial state while precessing about the  $z$  axis. An FID is observed by quadrature detection on the transverse plane.

## 1.5. FOURIER TRANSFORMATION AND ITS APPLICATIONS IN NMR

The FID is the sum of many time domain signals with different frequencies, amplitudes and phases. These time domain signals are detected and digitized during the signal acquisition period. In order to separate the individual signals and display them in terms of their frequencies (spectra), the time domain data (FID) are converted to frequency spectra by applying Fourier transformation, named after its discovery by French mathematician Joseph Fourier.

The questions to be addressed in this section include:

1. What are the properties of Fourier transformation useful for NMR?
2. What is the relationship between excitation bandwidth and pulse length in terms of the Fourier transformation?
3. What is quadrature detection and why is it necessary?

### 1.5.1. Fourier Transformation and Its Properties Useful for NMR

The Fourier transformation describes the connection between two functions with dependent variables such as time and frequency ( $\omega = 2\pi/t$ ), called a Fourier pair, by the relationship (Bracewell, 1986):

$$F(\omega) = \text{Ft}\{f(t)\} = \int_{-\infty}^{\infty} f(t)e^{-i\omega t} dt \quad (1.21)$$

$$f(t) = \text{Ft}\{F(\omega)\} = \int_{-\infty}^{\infty} F(\omega)e^{i\omega t} d\omega \quad (1.22)$$

Although there are many methods to perform Fourier transformation for the NMR data, the Cooley–Tukey fast Fourier Transformation algorithm is commonly used to obtain NMR spectra from FIDs combined with techniques such as maximum entropy (Sibisi *et al.*, 1984; Mazzeo *et al.*, 1989; Stern and Hoch, 1992) and linear prediction (Zhu and Bax, 1990; Barkhuusen *et al.*, 1985). For NMR signals described as an exponential function (or sine and cosine pair) with a decay constant  $1/T$ , the Fourier pair is the FID and spectrum with the forms of:

$$f(t) = e^{(i\omega_0 - 1/T)t} \quad (1.23)$$

$$F(\omega) = \text{Ft}\{f(t)\} = \int_{-\infty}^{\infty} e^{(i\omega_0 - 1/T)t} e^{-i\omega t} dt = \frac{i(\omega_0 - \omega) + (1/T)}{(\omega_0 - \omega)^2 + (1/T^2)} \quad (1.24)$$

which indicate that the spectrum is obtained by Fourier transformation of the FID and the frequency signal has a Lorentzian line shape. Some important properties of Fourier transformation useful in NMR spectroscopy are discussed below (Harris and Stocker, 1998):

1. *Linearity theorem.* The Fourier transform of the sum of functions is the same as the sum of Fourier transforms of the functions:

$$\text{Ft}\{f(t) + g(t)\} = \text{Ft}\{f(t)\} + \text{Ft}\{g(t)\} \quad (1.25)$$

This tells us that the sum of time domain data such as an FID will yield individual frequency signals after Fourier transformation.

2. *Translation theorem.* The Fourier transform of a function shifted by time  $\tau$  is equal to the product of the Fourier transform of the unshifted function and the factor  $e^{i\omega\tau}$ :

$$\text{Ft}\{f(t + \tau)\} = e^{i\omega\tau} \text{Ft}\{f(t)\} = e^{i2\pi\phi} \text{Ft}\{f(t)\} \quad (1.26)$$

This states that a delay in the time function introduces a frequency-dependent phase shift in the frequency function. A delay in the acquisition of the FID will cause a first-order phase shift in the corresponding spectrum (frequency-dependent phase shift, see section 4.96). This also allows the phase of a spectrum to be adjusted after acquisition without altering the signal information contained in the time domain data  $f(t)$  (FID). The magnitude representation of the spectrum is unchanged because integration of  $|\exp(i\omega\tau)|$  over all possible  $\omega$  yields unity. Similarly,

$$\text{Ft}\{f(\omega - \omega_0)\} = e^{i\omega_0\tau} f(t) \quad (1.27)$$

A frequency shift in a spectrum is equivalent to an oscillation in the time domain with the same frequency. This allows the spectral frequency to be calibrated after acquisition.

3. *Convolution theorem.* The Fourier transform of the convolution of functions  $f_1$  and  $f_2$  is equal to the product of the Fourier transforms of  $f_1$  and  $f_2$ :

$$\text{Ft}\{f_1(t) * f_2(t)\} = \text{Ft}[f_1(t)] * \text{Ft}[f_2(t)] \quad (1.28)$$

in which the convolution of two functions is defined as the time integral over the product of one function and the other shifted function:

$$f_1(t) * f_2(t) = \int_{-\infty}^{\infty} f_1(\tau) f_2(t - \tau) d\tau \quad (1.29)$$

Based on this theorem, desirable line shapes of frequency signals can be obtained simply by applying a time function to the acquired FID prior to Fourier transformation to change the line shape of the spectral peaks, known as apodization of the FID.

4. *Scaling theorem.* The Fourier transform of a function with which a scaling transformation is carried out ( $t \rightarrow t/c$ ) is equal to the Fourier transform of the original function with the transformation  $\omega \rightarrow c\omega$  multiplied by the absolute value of factor  $c$ :

$$\text{Ft}\{f(t/c)\} = |c| F(c\omega) \quad (1.30)$$

According to this theorem, the narrowing of the time domain function by a factor of  $c$  causes the broadening of its Fourier transformed function in frequency domain by the same factor, and vice versa. This theorem is also known as similarity theorem.

5. *Parseval's theorem.*

$$\int_{-\infty}^{\infty} |f(t)|^2 dt = \int_{-\infty}^{\infty} |F(v)|^2 dv = \int_{-\infty}^{\infty} |F(\omega)|^2 d\omega \quad (1.31)$$

This theorem indicates that the information possessed by the signals in both time domain and frequency domain is identical.

### 1.5.2. Excitation Bandwidth

In order to excite the transitions covering all possible frequencies, the excitation bandwidth is required to be sufficiently large. This requirement is achieved by applying short RF pulses. In certain other situations, the excitation bandwidth is required to be considerably narrow to excite a narrow range of resonance frequencies such as in selective excitation. The following relationships of Fourier transform pairs are helpful in understanding the process.

A Dirac delta function  $\delta(t - \tau)$  in the time domain at  $t = \tau$  gives rise to a spectrum with an infinitely wide frequency range and uniform intensity:

$$\text{Ft}\{\delta(t - \tau)\} = \int_{-\infty}^{\infty} \delta(t - \tau) e^{-i\omega t} dt = e^{-i\omega\tau} \quad (1.32)$$

which produces a frequency domain function with a perfectly flat magnitude at all frequencies because  $|e^{-i\omega\tau}| = 1$ . The  $\delta$  function can be considered as an infinitely short pulse centered at  $\tau$ . This infinitely short pulse excites an infinitely wide frequency range. When  $\tau$  equals zero, each frequency has the same phase. Equation (1.32) means that in order to excite a wide frequency range, the RF pulse must be sufficiently short. Alternatively, for selective excitation, a narrow range of frequency is excited when a long RF pulse is used. A  $\delta$  function in the frequency domain representing a resonance at frequency  $\omega_0$  with a unit magnitude has a flat constant magnitude in the time domain lasting infinitely long in time:

$$\text{Ft}\{e^{i\omega_0 t}\} = \int_{-\infty}^{\infty} e^{i\omega_0 t} e^{-i\omega t} dt = 2\pi\delta(\omega - \omega_0) \quad (1.33)$$

For a single resonance excitation, the RF pulse is required to be infinitely long. In practice, the short pulses are a few microseconds, which are usually called hard pulses, whereas the long pulses may last a few seconds, and are called selective pulses. Shown in Figure 1.8 are the Fourier transforms of the short and long pulses. The bandwidth of the short pulse may cover several kilohertz and the selectivity of a long pulse can be as narrow as several hertz. A Gaussian function is the only function whose Fourier transformation gives another same-type (Gaussian) function [Figure 1.8(d) and (h)]:

$$\text{Ft}\{e^{-t^2/\sigma^2}\} = \int_{-\infty}^{\infty} e^{-t^2/\sigma^2} e^{-i\omega t} dt = -\sigma\sqrt{\pi}e^{-(\omega^2\sigma^2)/4} \quad (1.34)$$

A Gaussian shaped pulse will selectively excite a narrow frequency range. The value of  $\sigma$  determines the selectivity of the pulse. The broadening of a Gaussian pulse results in narrowing in the frequency domain. More details on selective shaped pulses will be discussed in Chapter 4.

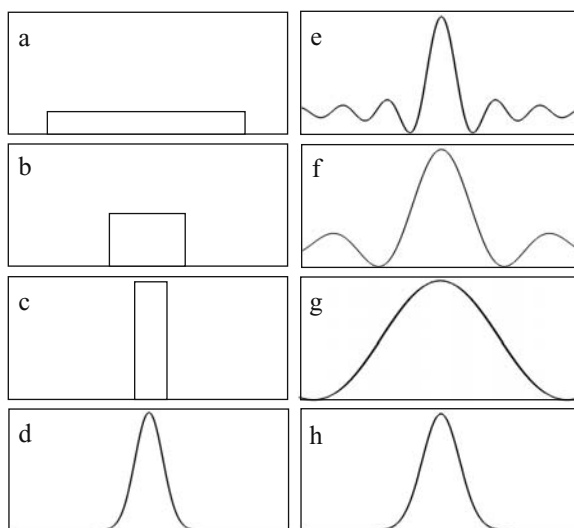


**Figure 1.8.** RF pulses and their Fourier transforms. Long and short rectangular pulses (a)–(c) and corresponding Fourier transforms (e)–(g), Gaussian shaped pulse (d) and its Fourier transform (h).

### 1.5.3. Quadrature Detection

Two important time domain functions in NMR are the cosine and sine functions. The Fourier transformations of the two functions are as follows:

$$\text{Ft}\{\cos(\omega_0 t)\} = \int_{-\infty}^{\infty} \frac{1}{2} (e^{i\omega t} + e^{-i\omega t}) e^{-i\omega t} dt = \frac{1}{2} [\delta(\nu - \nu_0) + \delta(\nu + \nu_0)] \quad (1.35)$$

$$\text{Ft}\{\sin(\omega_0 t)\} = \int_{-\infty}^{\infty} \frac{1}{2i} (e^{i\omega t} - e^{-i\omega t}) e^{-i\omega t} dt = \frac{1}{2i} [\delta(\nu - \nu_0) - \delta(\nu + \nu_0)] \quad (1.36)$$

The time domain signal may be considered as a cosine function. If an FID is detected by a single detector in the  $xy$  plane in the rotating frame during acquisition after a  $90^\circ$  pulse, the Fourier transformation of the cosine function gives rise to two frequency resonances located at  $\nu_0$  and  $-\nu_0$ , as described by the  $\delta$  functions in Equation (1.35). This indicates that the time domain signal detected by a single detector does not have information on the sign of the signal. As a result, each resonance will have a pair of peaks in the frequency domain. In order to preserve the information on the sign of the resonance, a second detector must be used, which is placed perpendicular to the first one in the  $xy$  plane. The signal detected by the second detector is a sine function (a time function which is  $90^\circ$  out of phase relative to the cosine function). The combined signal detected by the quadrature detector is a complex sinusoidal function,  $e^{i\omega_0 t}$ , which produces a resonance at  $\omega_0$  or  $\nu_0$ :

$$\text{Ft}\{e^{i\omega_0 t}\} = \int_{-\infty}^{\infty} e^{i\omega_0 t} e^{-i\omega t} dt = 2\pi \delta(\omega - \omega_0) = \delta(\nu - \nu_0) \quad (1.37)$$

Therefore, quadrature detection (two detectors aligned perpendicularly) is required to detect NMR signals with a distinguishable sign in the frequency domain.

## 1.6. NYQUIST THEOREM AND DIGITAL FILTERS

Questions to be addressed in the current section include:

1. What is the Nyquist theorem and how does it affect NMR signal detection?
2. What is the relationship between the spectral window (SW) and the sampling rate of detection?
3. What is digital filtering and its application to NMR?

In the analog-to-digital conversion of the NMR signal, the analog signal is sampled with a certain sampling rate by the ADC (analog-to-digital converter, Chapter 2). The Nyquist theorem (Bracewell, 1986) states that for the frequency to be accurately represented the sampling rate is required to be at least twice the frequency. In other words, the highest frequency which can be accurately sampled is half of the sampling rate. This frequency is called the Nyquist frequency, which is defined as the spectral width, or the spectral window (SW). As a result, two time points must be recorded per period of a sinusoidal signal. The time interval of sampling is called the dwell time (DW) and  $1/DW$  is the sampling rate, which based on the Nyquist theorem has the relationship with SW:

$$f_n = SW = \frac{1}{2DW} \quad (1.38)$$

If a signal frequency,  $\nu$ , is higher than the Nyquist frequency, it will appear at a different frequency in the spectrum, called an aliasing frequency:

$$\nu_a = \nu - kf_n \quad (1.39)$$

in which  $\nu$  is the frequency of the signal,  $f_n$  is the Nyquist frequency,  $\nu_a$  is the aliased frequency and  $k$  is an integer. For example, if the spectral width is set to 8 kHz, a signal with frequency 9 kHz will appear at 1 kHz. A signal with a frequency outside the SW can also be folded into the spectrum, called the folded frequency. For an  $f_n$  of 8 kHz, for instance, a signal with frequency 9 kHz will be folded at 7 kHz. Usually, a folded peak in an NMR spectrum shows a different phase than the unfolded peaks. In order to remove the aliased or folded signals, analog filters can be utilized before the signal is digitized. However, frequencies beyond the pass band (including noise) can still appear in the spectrum as the folded or aliased frequencies because the transition band between the pass band and stop band of analog filters is rather large (see Figure 1.9 for the definition of the transition band, pass band, and stop band of a filter). The real solution to avoid folding-in of signals and noise is to utilize digital filters combined with oversampling (Winder, 1997; Moskau, 2001).

Oversampling denotes that the time domain signal is acquired using a larger spectral width and a larger number of data points than necessary. Because the spectral width is determined by the sampling rate (Nyquist theorem), 10-fold oversampling increases both the spectral width and the number of data points by 10 times (whereas the acquisition time is not changed). The role of the oversampling is to reduce the “quantization noise” produced by the ADC in



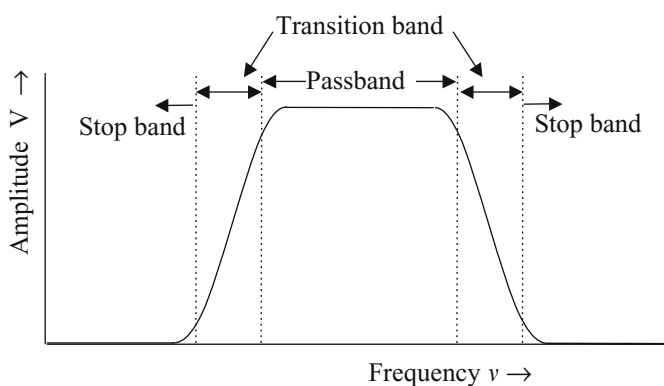


**Figure 1.9.** Characterization of a bandpass filter. The signals with frequencies inside the pass band of the filter pass through the filter, while those with frequencies in the stop band are filtered out. The amplitudes of the signals with frequencies inside the transition band are attenuated (Winder, 1997).

the case that the receiver gain has to be set to a high value, by spreading the noise over the larger spectral width. As a result, the dynamic range as well as the signal-to-noise ratio can be increased. In addition, application of oversampling causes a flatter baseline of the spectrum. A significantly larger number of data points is generated by the oversampling, which requires much disk storage space. For example, 20-fold oversampling of 32 k data points will generate 640 k data points (k is equivalent to multiplying the number by 1024). To avoid the unnecessary larger data sets a real-time digital filter is used to reduce the spectral width to that of interest by removing the frequency range outside the desired spectral width before the data are stored on disk. The digital filtering is achieved by a digital signal processor integrated with the ADC circuits (real-time) before time averaging, or by software (post-acquisition) after the acquired FID is transferred from the console to the host computer prior to storage on disk.

Similar to analog filters, a digital filter is characterized by the pass band (SW of interest) and the shape of the stop band, which describes the steepness of the cutoffs of the filters (the stop band is the region to be filtered out, Figure 1.9). For post-acquisition filters, the steepness of the cutoff is determined by the number of coefficients. A larger number of coefficients defines a filter with sharper cutoffs and flatter pass band (brick-wall type with narrower transition band), whereas a smaller number of coefficients characterizes filters with slower cutoffs (wider transition band). The real-time digital filters can be characterized as two types: brick-wall type with sharpest cutoffs and analog-like with gradual cutoffs.

## 1.7. CHEMICAL SHIFT

From the previous sections, we know how a detectable magnetization is generated and how an FID is acquired with quadrature detection. Now, we would like to know what kind of signals we are going to observe and how the information can be used.

In the current section, questions will be addressed such as:

1. What is chemical shift?

2. Where does chemical shift originate?
3. What are the references and units of chemical shift?

All nuclear spins of the same isotope would have the same resonance frequency if there were no other kinds of interaction in addition to the Zeeman interaction. In fact, for a given isotope, dispersion of the NMR signals of nuclei is caused by the difference in the environment surrounding the nuclei. One of the factors causing the difference in frequency is the electronic shielding. The torque generated by the magnetic field also causes a precession of electrons around the magnetic field direction. The directional electronic precession produces a local magnetic field with a magnitude proportional to  $B_0$ , which shields some portion of the static field from the nuclei. This electronic precession is different from the random motion of electrons. The net effect can be described using a quality called the shielding constant  $\sigma$  by:

$$\nu = \frac{\gamma}{2\pi} B_0 (1 - \sigma) \quad (1.40)$$

The shielding constant is always less than 1 because the induced local magnetic field will not be larger than the applied magnetic field.

The absolute zero of chemical shift is the one obtained for a bare nucleus without electrons. Although the absolute value of the chemical shift may be obtained for bare nuclei such as protons, it is convenient to use a specific compound as a reference, whose resonance frequency is set to the chemical shift value of zero. The chemical shifts of other resonances are expressed as the difference in electron shielding to the reference nucleus:

$$\delta = \frac{\nu - \nu_{\text{ref}}}{\nu_{\text{ref}}} 10^6 \quad (1.41)$$

in which  $\nu$  and  $\nu_{\text{ref}}$  are the resonance frequencies of the nucleus under study and the reference nucleus in units of megahertz, respectively, and  $\delta$  is the chemical shift in units of ppm (parts per million) of the nucleus with frequency  $\nu$ . Chemical shift  $\delta$  is independent of magnetic field strength, that is, the resonances in ppm present in a spectrum remain the same when obtained at different magnets with different field strengths. The reference compound is required to have the following properties: (a) stability in a variety of solvents, (b) an unchanged chemical shift value over a wide range of temperature and pH values, and (c) ease of handling. Two compounds are commonly used for  $^1\text{H}$  NMR reference: tetramethylsilane (TMS), which is the standard reference adopted by the IUPAC (International Union of Pure and Applied Chemistry) and 2,2-dimethyl-2-silapentane-5-sulfonic acid (DSS), which is a secondary IUPAC reference (Harris *et al.*, 2001). Either of the reference compounds can be added into an NMR sample as an internal reference or used alone as an external reference. For internal referencing, the reference compound is dissolved with the sample, which clearly has limitations such as solubility, miscibility, or reaction with the sample. For external referencing, a reference compound is dissolved alone in a specific solvent and the chemical shift is measured for the reference either in its own NMR tube or in a capillary insert tube inside the sample NMR tube. The zero frequency is set to the resonance frequency of the reference nucleus, which is used for all other experiments with the same isotope. Because of the high stability and homogeneity of NMR spectrometers, the external reference is of practical use for biological samples. In fact, once the chemical shift reference is calibrated on a spectrometer, the reference frequency will not change unless the  $^2\text{H}$  lock frequency is adjusted. The gradual drift of the magnetic

field is corrected by the  $z_0$  current of the shimming assembly (see shimming and locking in Chapter 4).

TMS is commonly used as the reference in  $^1\text{H}$  and  $^{13}\text{C}$  spectra for samples in organic solvents. Chemical shifts for all isotopes should include two decimal digits. DSS is commonly chosen as  $^1\text{H}$  and  $^{13}\text{C}$  external references for biological samples, which is dissolved in water in a pH range of 2–11 and used at 25°C. The chemical shift of water or HDO has a temperature dependence that can be expressed as referenced to DSS over a wide temperature range:

$$\delta_{\text{H}_2\text{O}} \text{ (ppm)} = 4.76 - (T - 25)0.01 \quad (1.42)$$

For  $^{31}\text{P}$  NMR, 85%  $\text{H}_3\text{PO}_4$  is the IUPAC standard reference which can be used externally (with a capillary insert). The chemical shift reference for  $^{15}\text{N}$  is complicated and sometimes very confusing. Because there is no compound similar to DSS or TMS available for  $^{15}\text{N}$  referencing as in the case of  $^1\text{H}$  or  $^{13}\text{C}$ , a variety of reference systems have been used to define 0.00 ppm for  $^{15}\text{N}$ . Although  $\text{CH}_3\text{NO}_2$  is the IUPAC  $^{15}\text{N}$  reference, liquid  $\text{NH}_3$  is the most popular  $^{15}\text{N}$  reference for biological NMR. The disadvantage is the difficult handling of the sample. Indirect reference compounds are usually used such as  $^{15}\text{N}$  urea in dimethyl sulfoxide (DMSO) and saturated ammonium chloride in water.  $^{15}\text{N}$  urea in DMSO is a convenient sample as an indirect reference and has an  $^{15}\text{N}$  chemical shift of 78.98 ppm relative to liquid ammonium. It should be noted that an  $^{15}\text{N}$  urea reference sample must be locked at the frequency of  $^2\text{H}_2\text{O}$ . A simple method to achieve this is to place a capillary tube with  $^2\text{H}_2\text{O}$  inside the NMR tube of the urea sample. An alternative way to obtain the correct reference frequency using the  $^{15}\text{N}$  urea sample is to acquire the spectrum without  $^2\text{H}$  locking. After the lock frequency is set to be on the resonance of  $^2\text{H}_2\text{O}$  using a  $^2\text{H}_2\text{O}$  sample, the  $^{15}\text{N}$  urea sample is placed into the probe without altering the lock frequency. Shimming can be done with  $^2\text{H}$  gradient shimming. After setting the resonance frequency of  $^{15}\text{N}$  urea to 78.98 ppm, the frequency at 0.00 ppm is the reference frequency for  $^{15}\text{N}$  experiments in aqueous solutions.

Recently a more convenient referencing system has been introduced that uses the  $^1\text{H}$  reference for heteronuclei through the frequency ratio  $\Xi$  of the standard reference sample to DSS (or TMS):

$$\frac{\Xi}{\%} = 100 \frac{\nu_{\text{X}}}{\nu_{\text{DSS}}} \quad (1.43)$$

in which  $\nu_{\text{DSS}}$  and  $\nu_{\text{X}}$  are the observed  $^1\text{H}$  frequency of DSS and the observed frequency of X nucleus of the reference sample. The values of  $\Xi$  for different isotope reference samples are listed in Table 1.1. The reference frequency for X nuclei can be calculated from the  $^1\text{H}$  reference frequency on the spectrometer according to:

$$\nu_{\text{ref}}^{\text{X}} = \Xi_{\text{ref}} \nu_{\text{DSS}} = \frac{(\Xi_{\text{ref}}/\%) \nu_{\text{DSS}}}{100} \quad (1.44)$$

For example, if liquid  $\text{NH}_3$  is used as the  $^{15}\text{N}$  reference sample, the  $^{15}\text{N}$  reference frequency is given by:

$$\nu_{\text{ref}}^{^{15}\text{N}} = \frac{10.1329118 \nu_{\text{DSS}}}{100} \quad (1.45)$$

**TABLE 1.1**  
Frequency Ratio  $\Xi$  of Heteronuclear References

Nucleus	Reference compound	Sample condition	$\Xi/\%$	Literature
$^1\text{H}$	DSS	internal	100.000000	by definition
$^2\text{H}$	DSS	internal	15.3506088	Markley <i>et al.</i> , 1998
$^{13}\text{C}$	DSS	internal	25.1449530	Wishart <i>et al.</i> , 1995
$^{15}\text{N}$	Liquid $\text{NH}_3$	external	10.1329118	Wishart <i>et al.</i> , 1995
$^{31}\text{P}$	$(\text{CH}_3\text{O})_3\text{PO}$	internal	40.4808636	Markley <i>et al.</i> , 1998
$^{31}\text{P}$	$\text{H}_3\text{PO}_4$	external	40.4807420	Harris <i>et al.</i> , 2001

To set the reference frequency for heteronuclei, the  $^1\text{H}$  reference frequency  $\nu_{\text{DSS}}$  is first obtained for an aqueous sample containing DSS (1 mM). The chemical shift reference for heteronuclei is defined through the ratio  $\Xi$  according to Equation (1.44).

The reference frequency does not change if the spectrometer frequency is unchanged. Frequently, the spectrometer frequency is defined based on the deuterium lock frequency. Therefore, the lock frequency is kept unchanged during normal operation of the spectrometer. The calibrated reference is recorded corresponding to a lock frequency. It is good practice to keep a record of the spectrometer deuterium lock frequency when calibrating chemical shift references.

The shielding constant,  $\sigma$ , is dependent on the distribution of electron density surrounding the nucleus. Because the distribution generally is spherically asymmetrical,  $\sigma$  usually has an anisotropic value (chemical shift anisotropy, or CSA) with an orientational dependence. An NMR spectrum of a solid sample looks like the one shown in Figure 1.10 with a broad line width due to the orientation distribution of molecules in the sample. The broad chemical shift powder pattern can be averaged to its isotropic value,  $\sigma_{\text{iso}}$ , which is the trace of the three components of its chemical shift tensor, by mechanically rotating the sample about the direction along the magic angle,  $54.7^\circ$ , at a rate larger than the anisotropic line width, for example, 10 kHz:

$$\sigma_{\text{iso}} = \frac{\sigma_{xx} + \sigma_{yy} + \sigma_{zz}}{3} \quad (1.46)$$

The technique is well known as magic angle spinning, or in short, MAS. In solution, however, rapid molecular tumbling averages out the chemical shift anisotropy that the nuclei possess, resulting in sharp peaks at the isotropic resonances. If the molecular tumbling motion is slowed down, the anisotropic property can be restored in a solution sample, which contains rich information on molecular structures. Chemical shift anisotropy has been used in structure determination of proteins in both solid and solution samples.

Several factors can contribute to the shielding constant, one of which originates from a spherical electronic distribution (s orbital electrons) called diamagnetic shielding,  $\sigma_{\text{dia}}$  (Friebolin, 1993). The term diamagnetic indicates that the induced field has an opposite direction to the external static field,  $B_0$ . The shielding effect from a nonspherical electronic

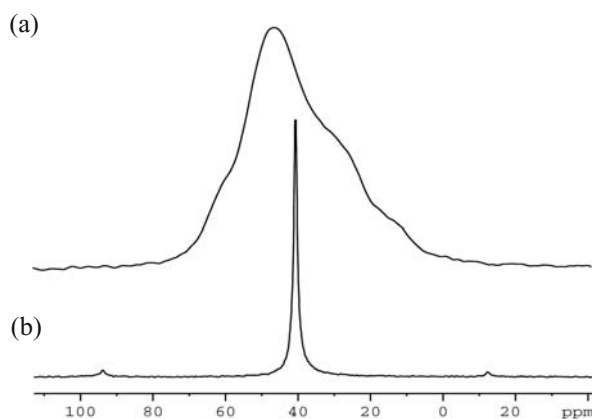


**Figure 1.10.** (a)  $^1\text{H}$  decoupled  $^{13}\text{C}$  powder pattern and (b) Magic-Angle-Spinning spectra of  $^{13}\text{C}_2\text{Glycine}$ .

distribution (electron orbitals other than the s orbital), in which the induced local field has the same direction as  $B_0$ , is called paramagnetic shielding,  $\sigma_{\text{para}}$ :

$$\sigma = \sigma_{\text{dia}} + \sigma_{\text{para}} \quad (1.47)$$

It should be noted that the term paramagnetic shielding has nothing to do with the effect of unpaired electrons, referred to as paramagnetic NMR spectroscopy. It is named for its opposite sign to the diamagnetic shielding. Because  $\sigma_{\text{dia}}$  and  $\sigma_{\text{para}}$  have opposite contributions to the shielding constant, some of the effects are canceled out. The contribution of  $\sigma_{\text{para}}$  is proportional to  $(m^2 \Delta E)^{-1}$  (the mass of the nucleus,  $m$ , and excitation energy to the lowest excited molecular orbital,  $\Delta E$ ) and the asymmetry of electronic distribution, whereas  $\sigma_{\text{dia}}$  is proportional to  $m^{-1}$  and the symmetry of electronic distribution. For protons, because the energy gap is large, the paramagnetic shielding is very small even when bonding causes distortion of the spherical distribution, resulting in a small shift range, normally 10 ppm. For  $^{13}\text{C}$ , the  $\sigma_{\text{para}}$  becomes an important contribution to the shielding because  $\Delta E$  is small. The distortion of the spherical electronic distribution induced by the bonding environment near the nuclei can significantly affect the value of the nuclear chemical shift. Hence,  $^{13}\text{C}$  has a wider range of chemical shifts (approximately 300 ppm) compared to  $^1\text{H}$  (Tables 1.2 and 1.3). The net effect of electronic precession produces a local magnetic field in the opposite direction to magnetic field  $B_0$ . Paramagnetic contributions usually have a dominant effect over the diamagnetic term in heteronuclei, which is responsible for the fact that the chemical shift range for heteronuclei is usually much larger than that of  $^1\text{H}$  (Table 1.2)

The other factor that contributes to the shielding constant is called the ring current effect (Lazzeretti, 2000), which arises from the delocalized electrons of the p orbital moving between bonded atoms in an aromatic ring. A classical example of the ring current is that the  $^1\text{H}$  chemical shift of benzene has a higher frequency (downfield shift) at 7.27 ppm compared to the resonance frequency of ethylene at 5.28 ppm. The  $\pi$  electrons of benzene circulating above and below the aromatic ring, when placed in a magnetic field, produce an additional magnetic field whose

**TABLE 1.2**  
Chemical Shift Range in Proteins and Peptides

Nucleus	NH <sup>backbone</sup>	NH <sup>sidechain</sup>	CH <sup>aromatic</sup>	C <sup>α</sup> H	C'	C <sup>β</sup> H
<sup>1</sup> H	8–10	6.5–8	6.5–8	3.5–5		1–4
<sup>13</sup> C			110–140	40–65	170–185	20–75
<sup>15</sup> N	110–140					

*Note:* <sup>1</sup>H and <sup>13</sup>C chemical shifts in parts per million are referenced to DSS, <sup>15</sup>N in parts per million is referenced to liquid NH<sub>3</sub> through its frequency ratio  $\Xi$ .

**TABLE 1.3**  
Average Chemical Shifts in Proteins and Peptides

Residue	<sup>1</sup> H <sup>N</sup>	<sup>15</sup> N	<sup>13</sup> C'	<sup>13</sup> C <sup>α</sup>	<sup>1</sup> H <sup>α</sup>	<sup>1</sup> H <sup>β</sup>	<sup>1</sup> H <sup>other</sup>
Ala	8.15	122.5	177.6	52.2	4.33	1.39	
Arg	8.27	120.8	176.6	56.0	4.35	1.89, 1.79	$\gamma$ CH <sub>2</sub> 1.70, $\delta$ CH <sub>2</sub> 3.32, NH 7.17, 6.62
Asn	8.38	119.5	175.6	52.7	4.74	2.83, 2.75	$\gamma$ NH <sub>2</sub> 7.59, 6.91
Asp	8.37	120.6	176.8	53.9	4.71	2.84, 2.75	
Cys	8.23	118.0	174.6	56.8	4.54	3.28, 2.96	
Gln	8.27	120.3	175.6	56.0	4.33	2.13, 2.01	$\gamma$ CH <sub>2</sub> 2.38, $\delta$ NH <sub>2</sub> 6.87, 7.59
Glu	8.36	121.3	176.6	56.3	4.33	2.09, 1.97	$\gamma$ CH <sub>2</sub> 2.31, 2.28
Gly	8.29	108.9	173.6	45.0	3.96		
His	8.28	119.1	174.9	55.5	4.60	3.26, 3.20	2H 8.12, 4H 7.14
Ile	8.21	123.2	176.5	61.2	4.17	1.90	$\gamma$ CH <sub>2</sub> 1.48, 1.19, $\gamma$ CH <sub>3</sub> 0.95, $\delta$ CH <sub>3</sub> 0.89
Leu	8.23	121.8	176.9	55.0	4.32	1.65	$\gamma$ H 1.64, $\delta$ CH <sub>3</sub> 0.94, 0.90
Lys	8.25	121.5	176.5	56.4	4.33	1.85, 1.76	$\gamma$ CH <sub>2</sub> 1.45, $\delta$ CH <sub>2</sub> 1.70, $\epsilon$ CH <sub>2</sub> 3.02, $\epsilon$ NH <sub>3</sub> <sup>+</sup> 7.52
Met	8.29	120.5	176.3	55.2	4.48	2.15, 2.01	$\gamma$ CH <sub>2</sub> 2.64, $\epsilon$ CH <sub>3</sub> 2.13
Phe	8.30	120.9	175.9	57.9	4.63	3.22, 2.99	2,6H 7.30, 3,5H 7.39, 4H 7.34
Pro	—	128.1	176.0	63.0	4.42	2.28, 2.02	$\gamma$ CH <sub>2</sub> 2.03, $\delta$ CH <sub>2</sub> 3.68, 3.65
Ser	8.31	116.7	174.4	58.1	4.47	3.88	
Thr	8.24	114.2	174.8	62.0	4.35	4.22	$\gamma$ CH <sub>3</sub> 1.23
Trp	8.18	120.5	173.6	57.6	4.66	3.32, 3.19	2H 7.24, 4H 7.65, 5H 7.17, 6H 7.24, 7H 7.50, NH 10.22
Tyr	8.28	122.0	175.9	58.0	4.55	3.13, 2.92	2,6H 7.15, 3,5H 6.86
Val	8.19	121.1	176.0	62.2	4.12	2.13	$\gamma$ CH <sub>3</sub> 0.97, 0.94

*Note:* The chemical shifts of <sup>1</sup>H, <sup>13</sup>C and <sup>15</sup>N are in parts per million, and referenced to DSS, DSS, and liquid NH<sub>3</sub>, respectively. The <sup>1</sup>H<sup>N</sup>, <sup>1</sup>H<sup>α</sup>, <sup>15</sup>N, and <sup>13</sup>C' are from Wishart *et al.* (1991), <sup>13</sup>C<sup>α</sup> are from Spera and Bax (1991), <sup>1</sup>H<sup>β</sup> and <sup>1</sup>H<sup>other</sup> are from Wüthrich (1986).

direction is opposite to the external static magnetic field at the center of the aromatic ring and along the external field at the outside edge of the ring. As a result, the field at the center of the ring has been reduced (more shielding), whereas the protons directly attached to the ring experience a field larger than the external field due to the addition of the induced field (deshielding). This phenomenon is called the ring current effect. The ring current has less effect on the <sup>13</sup>C chemical shifts of aromatic compounds. This has been explained by considering the fact that carbon nuclei are located approximately where the induced field changes direction between shielding and deshielding, that is, the induced field is close to zero.

## 1.8. NUCLEAR COUPLING

Electronic shielding is one of the nuclear interactions contributing to the resonance frequency of nuclei. Interactions other than chemical shift are entirely independent of magnetic field strength. These interactions provide information on the structures and dynamics of biological molecules.

Questions to be addressed in the current section include:

1. What is scalar coupling and where does it originate?
2. What is its magnitude range and how can it be measured?
3. How does scalar coupling provide information on molecular structure?
4. What is the nuclear dipolar interaction and where does it originate?
5. How is its magnitude characterized?
6. Where does the nuclear Overhauser effect (NOE) come from and how is it generated?
7. How does NOE provide information on molecular structure?
8. What is the residual dipolar interaction and why does it exist in a solution sample?

### 1.8.1. Scalar Coupling

Scalar ( $J$ , indirect, or spin–spin) coupling is the effect on nuclear spin A caused by the local magnetic field of its neighbor spin B. The orientation of spin B in the magnetic field produces a small polarization of the electrons mostly in the s orbital surrounding spin B. This polarization affects the electron density distribution of spin A directly bonded to spin B. Because the interaction depends on the s orbital electron density at the pair of nuclei, the electron density of the nuclei must be correlated, that is, in Fermi contact. Consequently,  $J$  coupling propagates only along chemical bonds.

Although  $J$  coupling is anisotropic due to the asymmetric environment surrounding the nuclear spin, the interaction is averaged to an isotropic value in solution by the rapid molecular tumbling motion. The magnitude of  $J$  coupling reduces significantly as the number of bonds separating the nuclei increases. Two-bond and three-bond couplings are at least one magnitude smaller than one-bond  $J$  couplings. Couplings longer than three bonds are close to zero, with an exception that long-range coupling beyond three bonds is observable in double-bonded compounds. Listed in Table 1.4 is the range of  $J$  couplings in different molecular bonds. When the frequency difference  $\Delta\nu$  in chemical shifts of spin  $I$  and  $S$  is much larger than the  $J$  coupling (weak coupling approximation,  $\Delta\nu \gg J$ ), all peaks have equal intensity. This gives rise to a first-order spectrum. When the frequencies of two coupled nuclei are closer in magnitude to the  $J$  coupling ( $\Delta\nu/J \leq 10$ ), second-order character will appear in the spectrum, which complicates the spectrum and produces uneven spectral intensities.

Homonuclear  $J$  coupling comes from interaction between nuclei with the same gyromagnetic ratio,  $\gamma$ , whereas heteronuclear  $J$  coupling comes from those with different  $\gamma$ . According to the Dirac vector model, the low energy state is that in which the magnetic moments of nuclei A and B are in antiparallel configuration to the magnetic moments of their bonding electrons (Figure 1.11). Since A and B are bonded, the electron of spin B in the bonding pair is also in antiparallel configuration with the electron of spin A. As a result, the nuclear spins A and B are antiparallel in the low energy state. If both A and B have positive gyromagnetic ratios such as in a CH bond, the effect of the coupling in which nuclei A and B are in antiparallel configuration stabilizes the low energy state, resulting in positive  $J$ . Another example is  $J$

**TABLE 1.4**  
Range of  $J$  Coupling Constants

	$J_{HH}$	$J_{CH}$	$J_{CC}$	$J_{NC}$	$J_{NH}$
$^1J$	276	120–250	30–80	<20	60–95
$^2J$	–30 to 0	–10 to 30	<20	<10	
$^3J$	<20	<10	<5	<1	

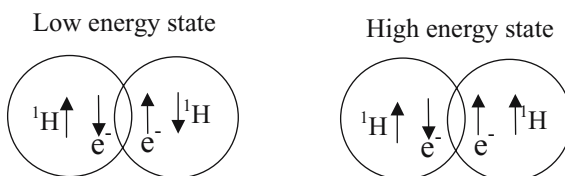


**Figure 1.11.** Dirac model for one-bond  $J$  coupling (two-spin system). When both nuclei A and B have the same sign of gyromagnetic ratio  $\gamma$ , the effect of the coupling in which nuclei A and B are in antiparallel configuration stabilizes the low energy state, resulting in positive  $J$ .

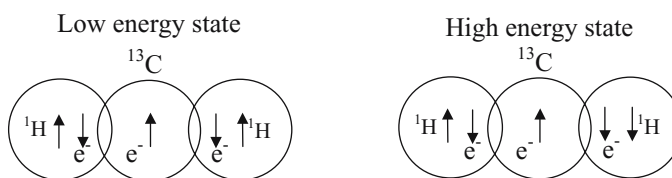


**Figure 1.12.** Dirac model for  $J$  coupling of geminal protons. Arrows represent nuclei or electrons as labeled. For homonuclear  $J$  coupling, the effect of the coupling in which two protons in the low energy state are in parallel configuration destabilizes the low energy state, resulting in negative  $J$ .

coupling between geminal protons as shown in Figure 1.12. The two geminal protons bond to a common carbon. In order to form a covalent bond, the electrons of two protons must be in antiparallel configuration with the electron of the carbon. The energy state in which both protons have antiparallel configuration with their own electron has low energy. Since the two protons in the low energy state have a parallel configuration to each other, the coupling of the two protons destabilizes the low energy state, leading to a negative  $J$  coupling.

Since only s orbital electrons at the pair of nuclei contribute to the  $J$  coupling according to the Fermi contact mechanism, one-bond scalar couplings depend on the fraction of s orbital electrons involved in the bonding. For instance, the one-bond  $J$  coupling constants between  $^1\text{H}$  and  $^{13}\text{C}$  or between  $^{13}\text{C}$  carbons are different for carbons with  $\text{sp}^3$ ,  $\text{sp}^2$ , and  $\text{sp}$  orbitals. Because an  $\text{sp}$  carbon has a 50% s fraction and an  $\text{sp}^3$  carbon has a 25% s fraction, ethyne has  $^1J_{\text{CH}}$  and  $^1J_{\text{CC}}$  couplings twice and 4-fold as large as those of methane, respectively (Table 1.5).

Heteronuclear coupling constants between two nuclear isotopes I and S will be indicated by subscripts as  $J_{\text{IS}}$ , for example,  $J_{\text{CH}}$  for the  $J$  coupling constant between  $^{13}\text{C}$  and  $^1\text{H}$ . For homonuclei, subscripts are used to indicate the position of coupled protons.  $^3J_{23}$  denotes the



**TABLE 1.5**  
Correlation of  $J$  Coupling with the Contribution of s Orbital Electrons

Bond	s Fraction in CH bond	$^1J_{CH}$	s Fraction in CC bond	$^1J_{CC}$
$CH_3-CH_3$	$25\% \times 100\%$	125	$25\% \times 25\%$	35
$CH_2=CH_2$	$33\% \times 100\%$	156	$33\% \times 33\%$	67
$CH\equiv CH$	$50\% \times 100\%$	249	$50\% \times 50\%$	171

vicinal coupling constant between protons at positions 2 and 3. The number of bonds between the coupled nuclei is indicated by a superscript number before  $J$ , for example,  $^2J_{HH}$  for the  $J$  coupling constant between two geminal protons and  $^3J_{HH}$  for a vicinal H–H coupling (three-bond). Sometimes the number is ignored in one-bond coupling constants such as  $J_{CH}$  or  $J_{NH}$ . Since there is no one-bond coupling between protons in proteins and polypeptides, the coupling between protons is much weaker than the one-bond coupling of protons with carbon, nitrogen, or other nuclear isotopes.

Three-bond H–H coupling constants  $^3J_{HH}$  contain information on the relative orientation of the coupled protons. Numerous studies have been performed to understand the relationship of coupling constants with dihedral angles. Karplus (1959) has theoretically described the dependence of the vicinal coupling constant  $^3J_{HH}$  on the dihedral angle formed by the vicinal protons:

$$^3J_{HH} = 8.5 \cos^2 \phi \quad \text{when } 0^\circ \leq \phi \leq 90^\circ \quad (1.48)$$

$$^3J_{HH} = 9.5 \cos^2 \phi \quad \text{when } 90^\circ \leq \phi \leq 180^\circ \quad (1.49)$$

The general Karplus equation can be written as:

$$^3J = A \cos^2 \theta + B \cos \theta + C \quad (1.50)$$

in which  $A$ ,  $B$ , and  $C$  are the constants which depend on the specific coupled nuclei and  $\theta$  is the dihedral angle (Karplus, 1963). Semiempirical methods have been used to obtain values of constants  $A$ ,  $B$ , and  $C$  by studying the correlations of observed  $^3J$  values to the dihedral angles in known protein structures. The relationship of  $^3J_{H^N H^\alpha}$  to the dihedral angle  $\phi$  has been derived from the structure of Ubiquitin (Wang and Bax, 1996):

$$^3J = 6.98 \cos^2 \theta - 1.38 \cos \theta + 1.72 \quad (1.51)$$

in which  $\theta = \phi - 60$ . It should be noted that as many as four possible dihedral values can be derived from the above equation, which is clearly visible in the corresponding Karplus curve in Figure 7.2 (Chapter 7). This ambiguity needs to be taken into account in the application of dihedral angle restraints in structure determination.

### 1.8.2. Spin Systems

The spin system refers to a group of nuclei that are coupled through  $J$  coupling. If a spin couples to one neighboring nucleus with a large chemical shift separation (weak coupling approximation,  $\Delta\nu \gg J$ ), the two-spin system is said to be an AX system. In contrast, when the frequencies of the two nuclei are on the same order of magnitude as  $J$  coupling ( $\Delta\nu \approx J$ ), the spin system is called an AB spin system, which has close chemical shifts. In the absence of  $J$  coupling, the frequencies of the transitions for an AX spin system formed by spin I and spin S as shown in Figure 1.13(a) are:

$$\begin{aligned} \nu_{12} &= \nu_S; & \nu_{34} &= \nu_S \\ \nu_{13} &= \nu_I; & \nu_{24} &= \nu_I \end{aligned}$$

In the presence of  $J$  coupling [Figure 1.13(b)], the frequencies become:

$$\begin{aligned} \nu_{12} &= \nu_S - \frac{1}{2}J_{IS}; & \nu_{34} &= \nu_S + \frac{1}{2}J_{IS} \\ \nu_{13} &= \nu_I - \frac{1}{2}J_{IS}; & \nu_{24} &= \nu_I + \frac{1}{2}J_{IS} \end{aligned}$$

Each of the two chemical shift resonances now is split into two lines with the same intensity separated by  $J$  Hz, producing four lines in the spectrum. In molecules, there will often be protons coupling to two or more equivalent vicinal protons through three bonds. For a proton weakly coupled to  $n$  equivalent protons, the spin system is denoted as  $AX_n$ . In an  $AX_n$  spin system, the number of split peaks and their relative intensities follow Pascal's triangle rule:

			1			$n = 0$
		1		1		$n = 1$
	1		2		1	$n = 2$
	1	3		3	1	$n = 3$
1		4	6	4		$n = 4$

in which each number represents a split peak and the value of the number indicates the relative intensity of the signal peak.

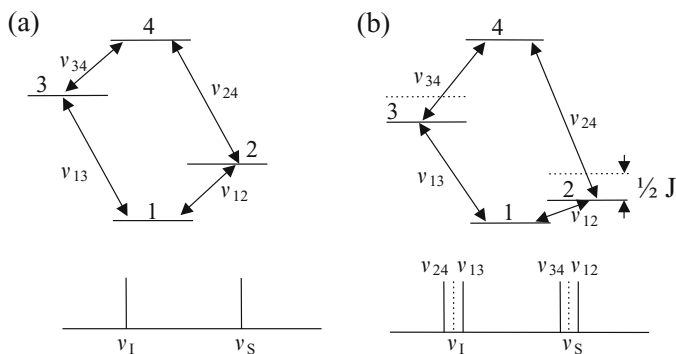


**Figure 1.13.** Standard energy diagrams and spectra of AX spin systems (a) without and (b) with  $J$  coupling. Frequencies  $\nu_{13}$  and  $\nu_{24}$  are the transitions of spin I, whereas  $\nu_{12}$  and  $\nu_{34}$  are those of spin S. The dashed lines in (b) represent the energy levels or frequency positions without  $J$  coupling.

### 1.8.3. Dipolar Interaction

Dipolar interaction plays an important role in structural and dynamic studies by NMR spectroscopy because of its dependence on the orientation and distance between dipole-coupled nuclei. In this section, the following questions will be addressed:

1. What is nuclear dipolar interaction?
2. How is the interaction described in equation form?
3. Where does NOE originate?
4. Under what conditions can the dipolar interaction be observed by solution NMR spectroscopy?

For weakly coupled spins, the dipolar contribution to the observed resonance in the high field limit is given by a simple orientation and distance dependence:

$$\nu_D = \nu_{\parallel} \frac{(3 \cos^2 \theta - 1)}{2} \quad (1.52)$$

in which  $\theta$  is the angle between the dipolar vector and the magnetic field (Figure 1.14) and  $\nu_{\parallel}$  is the magnitude of the dipolar vector, or dipolar coupling constant, which is given by:

$$\nu_{\parallel} = -\frac{\gamma_1 \gamma_2 h}{4\pi^2 r^3} \quad (1.53)$$

where  $h$  is Planck's constant, and  $r$  is the distance between spins 1 and 2 which have the gyromagnetic ratios of  $\gamma_1$  and  $\gamma_2$ , respectively. In the spectrum,  $\nu_D$  is the frequency shift caused by the dipolar coupling, whereas  $\nu_{\parallel}$  is the dipolar coupling when the dipolar vector is parallel to the magnetic field. The dipolar interaction between two nuclear spins occurs through space rather than through a molecular bond as in  $J$  coupling. The magnitude of the dipolar coupling for two protons separated by 3 Å is about 4.5 kHz, which is much larger than that of a  $J$  coupling. The dipolar coupling constant decreases rapidly with an increase of the dipole–dipole (DD) distance as a function of  $r^{-3}$ . In solution, dipolar splitting is not observable because the orientational term of the dipolar interaction with respect to the magnetic field direction is averaged to zero by rapid molecular tumbling. However, the effect of dipolar

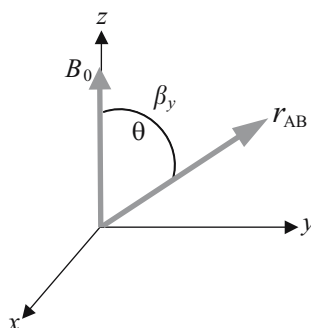


**Figure 1.14.** Relative orientation of the internuclear vector and magnetic field  $B_0$  in the laboratory frame.  $B_0$  is parallel to the  $z$  axis of the laboratory frame.

interaction on molecular relaxation still exists at any instant, which is the origin of the NOE. The DD interaction is the most important contribution to spin relaxation of molecules in solution.

#### 1.8.4. Residual Dipolar Coupling

Questions to be answered in this section include:

1. What is residual dipolar coupling (RDC) and how is it generated?
2. Why can RDC exist and how is it characterized?
3. How is the order of an alignment medium transferred to the macromolecules dissolved in the medium?
4. What are the requirements of the alignment media used to generate RDCs?

In a typical solution, the nuclear dipolar coupling is averaged to zero owing to rapid molecular tumbling. In the past several years, approaches have been developed to align macromolecules in solution with anisotropic media to regain the dipolar coupling (Tjandra and Bax, 1997; Prestegard *et al.*, 2000; de Alba and Tjandra, 2002; Lipstitz and Tjandra, 2004). Partial alignment of the macromolecules in media such as liquid crystals (Figure 1.15) leads to incomplete cancellation of the dipolar coupling, called residual dipolar coupling (RDC), which is the time or ensemble average of the dipolar coupling:

$$\nu_D = \nu_{\parallel} \frac{\langle 3 \cos^2 \Theta - 1 \rangle}{2} = \nu_{\parallel} \langle P_2(\cos \Theta) \rangle \quad (1.54)$$

in which angular brackets refer to averaging due to the molecular reorientations and internal motions,  $P_2(x) = (3x^2 - 1)/2$  is the second Legendre polynomial, and other parameters are defined as in Equations (1.52) and (1.53).

Since the dipolar interaction between heteronuclei is along the molecular bond, the sole unknown variable is the averaged molecular orientation,  $\Theta$ , of the dipolar interaction with respect to the laboratory frame and the magnetic field direction  $B_0$ . When the molecules are partially aligned in the magnetic field, the relative orientation of the dipolar interaction in the laboratory frame can be obtained by transforming the internuclear vector to an arbitrary molecular frame by angles  $\alpha_x$ ,  $\alpha_y$ , and  $\alpha_z$  between the  $x$ ,  $y$ , and  $z$  axes of the molecular frame and the vector. Then, the vector is further transformed from this molecular frame into the laboratory frame by a set of angles  $\beta_x$ ,  $\beta_y$ , and  $\beta_z$  between the  $x$ ,  $y$ , and  $z$  axes of the molecular frame and the magnetic field direction (the  $z$  axis of the laboratory frame, Figure 1.16). The angular dependence of the RDC can be represented by the two sets of angles as (Bax *et al.*, 2001):

$$\begin{aligned} \langle P_2(\cos \Theta) \rangle &= \frac{3}{2} \langle (\cos \alpha_x \cos \beta_x + \cos \alpha_y \cos \beta_y + \cos \alpha_z \cos \beta_z)^2 \rangle - \frac{1}{2} \\ &= \frac{3}{2} \langle (\cos^2 \alpha_x \cos^2 \beta_x + \cos^2 \alpha_y \cos^2 \beta_y + \cos^2 \alpha_z \cos^2 \beta_z \\ &\quad + 2 \cos \alpha_x \cos \alpha_y \cos \beta_x \cos \beta_y + 2 \cos \alpha_x \cos \alpha_z \cos \beta_x \cos \beta_z \\ &\quad + 2 \cos \alpha_y \cos \alpha_z \cos \beta_y \cos \beta_z) \rangle - \frac{1}{2} \end{aligned} \quad (1.55)$$

If  $c_{ij} = \cos \alpha_i \cos \alpha_j$  and  $C_{ij} = \cos \beta_i \cos \beta_j$  with  $i, j = (x, y, z)$ , Equation (1.55) can be rewritten as:

$$\langle P_2(\cos \Theta) \rangle = \frac{3}{2} \sum_{i,j=(x,y,z)} \langle C_{ij} c_{ij} \rangle - \frac{1}{2} \quad (1.56)$$

The variable  $C_{ij}$  is affected by the molecular tumbling, whereas  $c_{ij}$  is influenced by the internal motions. When the molecule is rigid,  $c_{ij}$  is not changed by the internal motions and then  $\langle C_{ij} c_{ij} \rangle = \langle C_{ij} \rangle c_{ij}$ . The equation of  $\langle P_2(\cos \Theta) \rangle$  becomes:

$$\langle P_2(\cos \Theta) \rangle = \sum_{i,j=(x,y,z)} S_{ij} c_{ij} \quad (1.57)$$

The  $3 \times 3$  matrix  $S$  is referred to as the Saupe order matrix, Saupe order tensor, or order tensor which is defined as:

$$S_{ij} = \frac{3}{2} \langle C_{ij} \rangle - \frac{1}{2} \delta_{ij} \quad (1.58)$$

in which  $\delta_{ij}$  is the Kronecker delta function. The Saupe order matrix is symmetric since  $\langle C_{ij} \rangle = \langle C_{ji} \rangle$ , and traceless ( $S_{xx} + S_{yy} + S_{zz} = 0$ ) because  $\sum \langle C_{ii} \rangle = 1$ . The symmetric condition eliminates three variables and the traceless condition reduces the final number of independent variables to five. In principle, if the molecular structure is known and hence  $c_{ij}$  is known, the five independent elements in the matrix can be obtained using the RDC for at least five internuclear vectors in the molecule, provided they are not parallel to the magnetic field. In practice, the number of measured dipolar couplings is much more than five.

More frequently, the orientational information contained in the equation is solved in a molecular axis system in which the order matrix is diagonal. This molecular axis system is called the principal axis system, in which the RDC is given by:

$$\nu_D(\alpha_x, \alpha_y, \alpha_z) = \nu_{\parallel} \sum_{i=(x,y,z)} S_{ii} c_{ii} \quad (1.59)$$

Now matrix  $S$  is a measurable quantity in the principal axis system because it is diagonal.  $S_{ii}$  also represents the probability of finding the  $i$ th axis along the magnetic field direction, which has the maximum value of 1 when the axis aligns with the magnetic field. The above equation tells us that the order information is contained in the order matrix and once the three elements of the order matrix in the principal axis system are known for a rigid molecule, the molecular structure may be determined by the RDC of the macromolecule. Equation (1.59) can also be represented in polar coordinates by using the relationships of  $c_{xx} = \sin^2 \theta \cos^2 \phi$ ,  $c_{yy} = \sin^2 \theta \sin^2 \phi$  and  $c_{zz} = \cos^2 \theta$  (Figure 1.16):

$$\nu_D(\theta, \phi) = \nu_{\parallel} (S_{xx} \sin^2 \theta \cos^2 \phi + S_{yy} \sin^2 \theta \sin^2 \phi + S_{zz} \cos^2 \theta) \quad (1.60)$$

in which  $\theta$  is the angle between the internuclear vector and the  $z$  axis of the molecular frame or the principal axis frame (Figure 1.16), which should not be confused with  $\theta$  in Equation (1.52) that defines the orientation of the nuclear vector with respect to  $B_0$  (Figure 1.14). In the

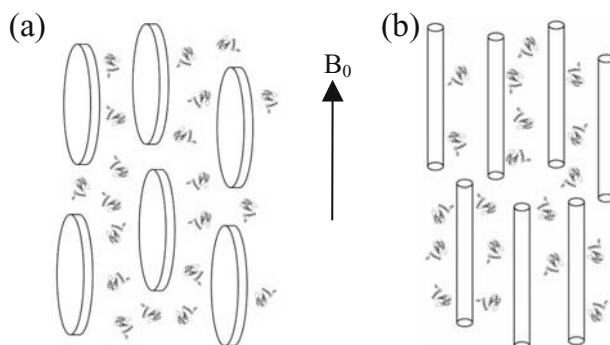


**Figure 1.15.** Alignment of biomolecules in two liquid crystal media (reproduced with permission from Tjandra, *Structure* 7, R205, 1999. Copyright © 1999 Elsevier). (a) Bicelles are believed to be disc-shaped pieces of lipid bilayers aligning with their bilayer normal perpendicular to the applied magnetic field  $B_0$ . (b) Rod-like particles represent filamentous phage aligning with their long axis parallel to  $B_0$ .

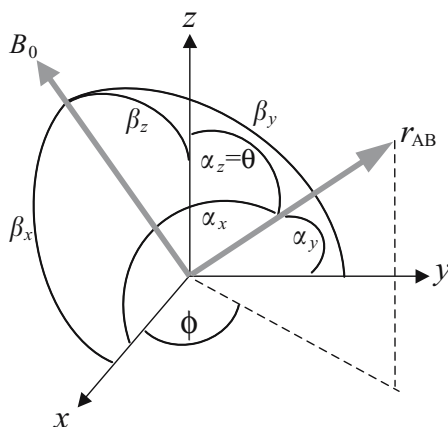


**Figure 1.16.** The relative orientations of the internuclear vector  $r_{AB}$  and  $B_0$  with respect to the  $x$ ,  $y$ , and  $z$  axes of the molecular frame. The orientation of the internuclear vector  $r_{AB}$  with respect to the molecular frame is defined by the  $\alpha$  angles, whereas the orientation of  $B_0$  with respect to the molecular frame is defined by the  $\beta$  angles.

principal axis system, only the differences in the principal values  $S_{kk}$  contribute to the RDC and the order tensor remains traceless ( $-S_{zz} = S_{xx} + S_{yy}$ ) with the most ordered axis  $|S_{zz}| > |S_{yy}| > |S_{xx}|$ . After rearranging the equation using the relationship of  $\cos^2 \phi = \frac{1}{2}(1 + \cos 2\phi)$ , and  $\sin^2 \phi = \frac{1}{2}(1 - \cos 2\phi)$ , the RDC is described as:

$$v_D(\theta, \phi) = v_{||} \left[ S_{xx} P_2(\cos \theta) + \frac{1}{2} (S_{xx} - S_{yy}) \sin^2 \theta \cos 2\phi \right] \quad (1.61)$$

By defining the principal alignment tensor  $A$  with an axial component  $A_a = S_{zz}$  and a rhombic component  $A_r = \frac{2}{3}(S_{xx} - S_{yy})$ , the RDC is rewritten as:

$$\nu_D(\theta, \phi) = \nu_{\parallel} \left[ A_a P_2(\cos \theta) + \frac{3}{4} A_r \sin^2 \theta \cos 2\phi \right] \quad (1.62)$$

In dilute liquid crystal media, the observed RDC is in the range of several hertz to several tens of hertz (0.1% of the dipolar coupling constant), meaning that the values of  $A_a$  are on the order of  $10^{-3}$ . The observed residual dipolar splitting is the difference of the two dipolar shifts, which is therefore given by:

$$\Delta \nu_D(\theta, \phi) = D_a \left[ (3 \cos^2 \theta - 1) + \frac{3}{2} R \sin^2 \theta \cos 2\phi \right] \quad (1.63)$$

in which  $D_a = A_a \nu_{\parallel}$  is the magnitude of the dipolar coupling normalized to the  $N-H$  dipolar coupling, and  $R = A_r/A_a$  is the rhombicity of the dipolar coupling. The residual dipolar splitting is sometimes written as:

$$\Delta \nu_D(\theta, \phi) = D_a [(3 \cos^2 \theta - 1) + \eta \sin^2 \theta \cos 2\phi] \quad (1.64)$$

in which  $\eta$  is the asymmetric parameter defined as  $\eta = (S_{xx} - S_{yy})/S_{zz}$  or  $\eta = \frac{3}{2}R$ . The residual dipolar splitting can be described according to Equation (1.60):

$$\Delta \nu_D(\theta, \phi) = D_{xx} \sin^2 \theta \cos^2 \phi + D_{yy} \sin^2 \theta \sin^2 \phi + D_{zz} \cos^2 \theta \quad (1.65)$$

in which  $D_{kk} = 2\nu_{\parallel} S_{kk}$  are the principal components of the RDC. The above equation resembles a powder pattern with three principal axes. It should be noted that the tensor  $D$  is also traceless, that is,  $D_{xx} + D_{yy} + D_{zz} = 0$ . They are related to  $D_a$  and  $R$  by the relationship:

$$D_{zz} = 2D_a \quad (\text{obtained when } \theta = 0^\circ, \phi = 0^\circ) \quad (1.66a)$$

$$D_{xx} = -D_a \left( 1 - \frac{3}{2} R \right) \quad (\text{when } \theta = 90^\circ, \phi = 0^\circ) \quad (1.66b)$$

$$D_{yy} = -D_a \left( 1 + \frac{3}{2} R \right) \quad (\text{when } \theta = 90^\circ, \phi = 90^\circ) \quad (1.66c)$$

When the molecular structure is known, the principal components  $A_a$  and  $A_r$  of the alignment tensor can be determined from the measured RDCs. However, when the molecular structure is not available, these components are estimated from the distribution of the observed RDCs (Figure 1.17). Because the magnitudes of the dipolar couplings are different for different types of internuclear bonds, it is necessary to normalize the observed residual couplings to the  $N-H$  dipolar coupling by scaling the observed dipolar coupling between nuclei  $i$  and  $j$  by a factor defined as  $\gamma_N \gamma_H r_{ij}^3 / \gamma_i \gamma_j r_{NH}^3$  in order to take into account all dipolar couplings together. The distribution of the observed dipolar couplings can be obtained by plotting the histograms of all normalized dipolar couplings as shown in Figure 1.17. For macromolecules, the histogram displays the powder pattern corresponding to that described by Equation (1.65). Therefore, the alignment tensor elements  $A_a$  and  $R$  can be estimated from the singularities of residual

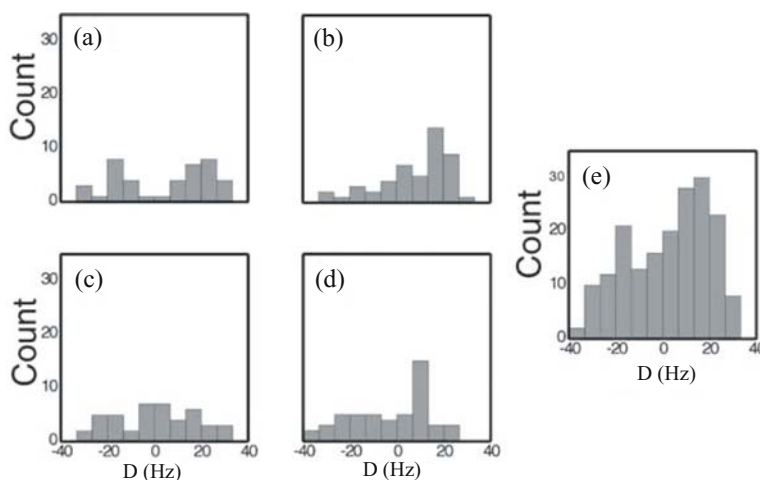


**Figure 1.17.** Histograms of normalized residual dipolar couplings (RDCs) of (a)  $^1\text{D}_{\text{NH}}$ , (b)  $^1\text{D}_{\text{C}^\alpha\text{H}^\alpha}$ , (c)  $^1\text{D}_{\text{C}^\beta\text{N}}$ , (d)  $^1\text{D}_{\text{NH}}$ . Because of the insufficient number of dipolar couplings, none of the individual types of dipolar couplings provides a powder pattern. (e) The addition of all the normalized dipolar couplings resembles a good powder pattern distribution (reproduced with permission from Baber *et al.*, *J. Mol. Biol.* 289, 949, 1999. Copyright © 1999 Elsevier).

dipolar splittings shown in the histogram. The estimated values are further optimized during the structural calculation by grid-searching the dipolar energy force as a function of the alignment tensor elements  $A_a$  and  $R$ .

From Equation (1.63) it is clear that each observed RDC produces two or more oppositely oriented cones of possible internuclear vector orientations. For an asymmetric alignment tensor, possible bond orientations on as many as eight sets of cones can be obtained from each dipolar coupling. This ambiguity makes it very difficult to determine the unique internuclear vector orientation without additional structural information. The degeneracy of the vector orientations can be reduced when two or more alignment tensors are obtained in different alignment media. A different alignment medium provides a different principal axis system, resulting in a different alignment tensor and thus resulting in a different set of orientation cones for a given dipolar coupling. The angle at the interception between two cones defined by the two alignment tensors yields the orientation of the internuclear vector.

## 1.9. NUCLEAR OVERHAUSER EFFECT

When the resonance of a spin in an NMR spectrum is perturbed by saturation or inversion of the magnetization, it may cause the spectral intensities of other resonances in the spectrum to change. This phenomenon is called the nuclear Overhauser effect or NOE. The intensity change caused by NOE originates from the population changes of the Zeeman states of coupled spins after perturbation through the dipolar interaction. The origin of a steady-state NOE can be clearly illustrated for a two-spin- $\frac{1}{2}$  system, in which the two spins are coupled by dipolar interaction but there is no  $J$  coupling between the spins (Solomon, 1955). Because the populations of spin states are changed by NOE, it is necessary to look at the process of change in population in order to understand the effect.



The energy diagram for the two-spin system contains four energy states as shown in Figure 1.18. The two spins are coupled via a dipolar interaction. For simplicity, the  $J$  coupling of the two spins is assumed to be zero. The resonance frequency of spin S is saturated by continuous radiation, which is denoted by transitions S of energy states  $\alpha\alpha \rightarrow \alpha\beta$  and  $\beta\alpha \rightarrow \beta\beta$ . The energy states are labeled in such a way that the first state represents that for spin S and the second for spin I. For example,  $\alpha\beta$  indicates that spin S is in state  $\alpha$  and spin I in state  $\beta$ . To simplify the notation, the four energy levels are denoted as 1 to 4 with the lowest energy level being named as 1. Therefore, there are two S ( $1 \rightarrow 2, 3 \rightarrow 4$ ) and two I transitions ( $1 \rightarrow 3, 2 \rightarrow 4$ ). Because  $J$  coupling is absent between the two spins, the two transitions for spin I have the same resonance frequency, yielding a singlet in the NMR spectrum, as do the two transitions of spin S. Since in general the chemical shifts are different for the two spins in either homonuclear or heteronuclear system, the resonances of spins I and S do not overlap.

Upon saturating transitions of spin S, the population of level 1 is equal to that of 2 and levels 3 and 4 have equal populations. As a result, levels 1 and 3 are less populated compared to the equilibrium whereas the populations at levels 2 and 4 are increased by saturation of the spin S resonance. After the irradiation, the system will try to restore equilibrium through all allowable relaxation processes. The normal spin-lattice relaxation (see section 1.10.2), labeled as  $w_1$ , does not alter the population difference for spin S because the two transitions have the same relaxation rate, resulting in no change in population difference between the spin states. Therefore, the relaxation  $w_1$  cannot change the intensity of spin I. However, in addition to spin-lattice relaxation via the above single-quantum transition there exist two other relaxation processes:  $w_0$  via a zero-quantum transition with  $\Delta m = 0$  and  $w_2$  via a double-quantum transition with  $\Delta m = 2$ . Although these transitions are not directly observable in the NMR spectrum since both are forbidden according to the selection rule (see section 1.2.2), they are allowed pathways for spin relaxations, known as cross-relaxation, which is the relaxation caused by an exchange of magnetization between spins. The system perturbed by saturation will try to relax via these relaxation pathways to get back to equilibrium. These relaxations are governed primarily by nuclear DD interaction. In other words, they exist only when the two spins are close to each other and coupled by the dipolar interaction. Either of the two relaxation processes changes the intensity of spin I. Whether the intensity is enhanced or reduced after saturation depends on which relaxation mechanism is dominant.

Assuming that the equilibrium populations are 1, 0, 0, and  $-1$  at energy levels 1–4, respectively, the populations are changed by the saturation to  $\frac{1}{2}, \frac{1}{2}, -\frac{1}{2}$ , and  $-\frac{1}{2}$  [Figure 1.18(b)]. The fractions represent the relative populations to those at level 2 or 3 at equilibrium state, which are set to zero for simplicity. When the perturbed system relaxes back to equilibrium via  $w_0$  alone, the populations at levels 2 and 3 eventually reach their equilibrium number, yielding the population distribution of  $\frac{1}{2}, 0, 0, -\frac{1}{2}$ . If it is observed and measured now, the intensity of spin I is reduced because the population difference for transitions  $1 \rightarrow 3$  and  $2 \rightarrow 4$  is decreased to  $\frac{1}{2}$  from 1 at the initial equilibrium state. As a consequence, the intensity of spin I corresponding to the transitions is reduced by  $w_0$  relaxation. On the other hand, if the system tries to relax via the  $w_2$  relaxation pathway the final populations at level 1 and 4 reach their equilibrium value but those of levels 2 and 3 do not relax, resulting in populations of 1,  $\frac{1}{2}, -\frac{1}{2}, -1$  for levels 1–4, respectively. Now the population difference for transitions  $1 \rightarrow 3$  and  $2 \rightarrow 4$  is increased to  $1\frac{1}{2}$  from the equilibrium value of 1. Hence, the enhanced intensity by NOE can be observed.

Which of the cross-relaxation pathways is favorable in a system depends on the rate of molecular motion in solution, or the correlation time of molecules. For the dipolar interaction

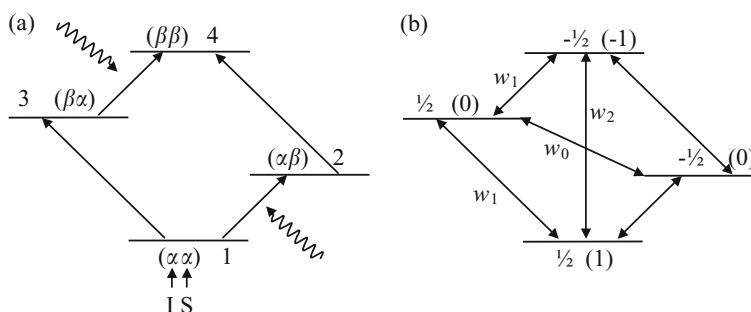


**Figure 1.18.** Standard energy diagram for a two-spin system with  $J_{IS} = 0$ . (a) The four states are labeled as 1 to 4 corresponding to  $\alpha\alpha$ ,  $\beta\alpha$ ,  $\alpha\beta$ , and  $\beta\beta$ , respectively. The two S transitions of  $1 \rightarrow 2$  and  $3 \rightarrow 4$  have equal frequencies, as do the I transitions of  $1 \rightarrow 3$  and  $2 \rightarrow 4$ . The S transitions are saturated by continuous RF irradiation at the resonance frequency of spin S. (b) The probabilities for zero-, single-, and double-quantum transitions are represented by  $w_0$ ,  $w_1$ , and  $w_2$ , respectively. The numbers in parentheses indicate the relative initial populations of energy levels, whereas the fractions are the populations after the saturation.

to cause cross-relaxations, the local field produced by the dipolar interaction must fluctuate at a rate in the same scale as the frequency corresponding to the transition to be relaxed. It is easy to see from the energy diagram in [Figure 1.18(b)] that the frequency corresponding to  $w_2$  relaxation is in the megahertz range of the Larmor frequency, whereas that corresponding to  $w_0$  is in the range of hertz to kilohertz because of the small energy gap for the transition. For small molecules which are tumbling fast at the frequency range of megahertz,  $w_2$  is the dominant relaxation, resulting in observed intensity enhancement—positive NOE. On the other hand, large biological molecules tumbling slowly produce a local field fluctuating at the frequency range of hertz to kilohertz and hence favor  $w_0$  relaxation, causing intensity reduction, that is, negative NOE. For medium sized molecules, the two relaxation pathways are competing in the system. When they are compatible, causing crossover between regimes such as for molecules with molecular weights of 1,000–3,000, the NOE is very weak, if not zero.

The NOE enhancement factor is limited by the ratio of the cross-relaxation rate to the total relaxation rate of spin I:

$$\eta = \frac{\gamma_S}{\gamma_I} \frac{w_2 - w_0}{2w_1 + w_2 + w_0} \quad (1.67)$$

in which  $\gamma_S$  and  $\gamma_I$  are the gyromagnetic ratios of spin S and spin I, respectively, the term  $(w_1 + w_2 + w_0)$  describes the total relaxation rate or dipolar spin-lattice relaxation, and  $(w_2 - w_0)$  is the cross-relaxation rate. The enhancement factor  $\eta$  can also be described by the intensities of spin I in the absence of the saturation,  $I_0$ , and in the presence of the saturation,  $I$ :

$$\eta = \frac{I - I_0}{I_0} \quad (1.68)$$

and the enhanced intensity is given by:

$$I = I_0(1 + \eta) \quad (1.69)$$

For small molecules with short correlation times (extremely narrowing limit),  $w_0 = 0$ , (see section 1.10.1), the maximum enhancement factor,  $\eta_{\max}$ , can be expressed in terms of the gyromagnetic ratios of the two spins (Neuhaus and Williamson, 1989):

$$\eta_{\max} = \frac{\gamma_S}{2\gamma_I} \quad (1.70)$$

Based on the above equation the maximum NOE enhancement obtained for small molecules in a homonuclear system is a factor of 0.5. For heteronuclear NOEs, the maximum factor is 1.99 for  $^{13}\text{C}-^1\text{H}$  ( $I = ^{13}\text{C}$ ,  $S = ^1\text{H}$ ) and 2.24 for  $^{31}\text{P}$ . For  $^{15}\text{N}$  observation, the sign of the NOE enhancement is reversed compared to  $^{13}\text{C}$  and  $^{31}\text{P}$ , due to the negative gyromagnetic ratio, which generates an enhancement factor of  $-4.94$ . On the other hand, for large molecules with long correlation times (spin diffusion limit),  $\eta_{\max}$  is limited by:

$$\eta_{\max} = -\frac{\gamma_S}{\gamma_I} \quad (1.71)$$

Therefore, in large molecules, nuclei with positive gyromagnetic ratios give rise to negative NOEs. For instance, homonuclear NOE enhancement in large molecules is  $-1.0$ , and heteronuclear  $^{13}\text{C}-^1\text{H}$  and  $^{31}\text{P}-^1\text{H}$  have twice the magnitude relative to small molecules,  $-3.98$  and  $-4.48$ , respectively. The  $^{15}\text{N}-^1\text{H}$  NOE enhancement in biomolecules is nearly 10-fold, at 9.88.

## 1.10. RELAXATION

The macroscopic magnetization  $M_0$  along the  $z$  axis of the rotating frame is rotated onto the  $y$  axis after a  $90^\circ_x$  pulse. The transverse magnetization will find ways to return to the  $z$  axis, which is its equilibrium state in the presence of the static magnetic field,  $B_0$ . In this section, the questions to be addressed are regarding such issues in spin relaxations as:

1. What is the correlation time and how is it related to spin relaxation?
2. What are the autocorrelation function and the spectral density function, and their relationship?
3. What are  $T_1$  and  $T_2$  relaxations and where do they originate?
4. How can they be characterized?
5. How can they be determined experimentally?

The nuclear relaxation from excited states back to the ground states in the presence of a magnetic field undergoes different mechanisms than emission relaxation in optical spectroscopy because the spontaneous and stimulated emissions for the nuclear system are much less efficient relaxations, in that the resonance frequencies are several orders of magnitude smaller compared to those in optical spectroscopy. The magnetization perturbed by RF pulses relaxes back to thermal equilibrium magnetization via two types of processes:  $T_1$  relaxation along the static magnetic field direction and  $T_2$  relaxation in the transverse plane perpendicular to the field direction (Abragam, 1961). The former is a result of nuclear coupling to the surroundings, which is characterized by spin-lattice or longitudinal relaxation time, whereas the latter is due to coupling between nuclei, which is characterized by the spin-spin or transverse

relaxation time. During  $T_1$  relaxation, the nuclei exchange energy with their surrounding or lattice, whereas there is no energy exchange with the lattice during  $T_2$  relaxation. Compared to the electrons, nuclear relaxation is very slow, which is on the order of milliseconds to hours.

### 1.10.1. Correlation Time and Spectral Density Function

Although the DD interaction is averaged to zero in solution, the field of the DD interaction is not zero at any given instant. The nuclear relaxations are essentially caused by fluctuating interactions. The strength of the fluctuating field is measured by the autocorrelation function  $G(\tau)$ , which is the time average of the correlation between a field measured at time  $t$  and the same field measured at time  $(t + \tau)$  (Neuhaus and Williamson, 1989):

$$G(\tau) = \overline{f(t)f(t + \tau)} \quad (1.72)$$

in which the bar represents time averaging.  $G(\tau)$  rapidly decays to zero as  $\tau$  increases. For isotropic rotational diffusion of a rigid rod with a spherical top, the decay is frequently assumed to be exponential with a time constant  $\tau_c$ . With this assumption, the autocorrelation function is reduced to:

$$G(\tau) = \frac{e^{(-\tau/\tau_c)}}{5} \quad (1.73)$$

in which  $\tau_c$  is the decay time constant of the autocorrelation function, called the correlation time, that is defined as the mean time between reorientation or repositioning of a molecule. The correlation time is used to describe the rate of random motions and is expressed as the average time between collisions for translational motions or the time for a molecule to rotate one radian in rotational motion. Frequently, expressing the fluctuation of the field as a function of frequency is of interest. Then, Fourier transformation of the autocorrelation function gives the correlation as a function of frequency known as the spectral density function:

$$J(\omega) = \int_{-\infty}^{\infty} G(\tau) d\tau = \int_{-\infty}^{\infty} \frac{e^{(-\tau/\tau_c)}}{5} e^{-i\omega\tau} d\tau = \frac{2}{5} \frac{\tau_c}{(1 + \omega^2 \tau_c^2)} \quad (1.74)$$

which is a Lorentzian function. As shown in Figure 1.19,  $J(\omega)$  is unchanged when  $\tau_c \omega \ll 1$  and decreases rapidly when  $\tau_c \omega \approx 1$ . The relationship between the autocorrelation function and the spectral density function is similar to that between an FID consisting of a single exponential decay and its Fourier transformed spectrum. Similar to autocorrelation function  $G(\tau)$ ,  $J(\omega)$  measures the strength of the fluctuating field in the frequency domain.

### 1.10.2. Spin-Lattice Relaxation

The nuclear relaxations are essentially caused by fluctuating interactions. The spin-lattice relaxation time  $T_1$  describes the recovery of  $z$  magnetization to its thermal equilibrium at which populations of the energy states reach the Boltzmann distribution. During  $T_1$  relaxation, exchange of energy with the environment (“lattice”) occurs due to various intra- and intermolecular interactions, including DD relaxation ( $T_1^{\text{DD}}$ ), chemical shift anisotropy ( $T_1^{\text{CSA}}$ ),

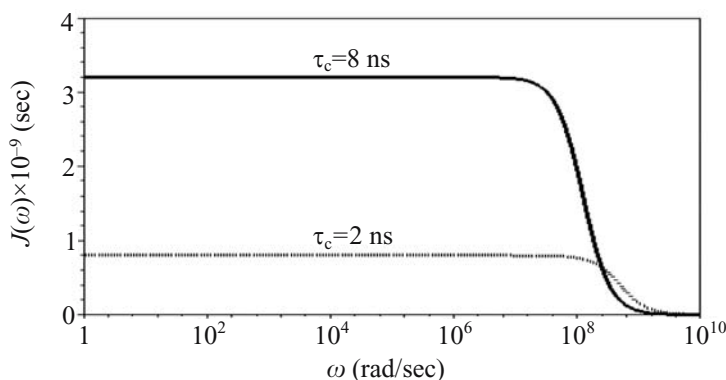


**Figure 1.19.** Spectral density functions for an isotropic rotor with  $\tau_c$  values of 2 ns (dotted line) and 8 ns (solid line) using Equation (1.74).

spin-rotation relaxation ( $T_1^{\text{SR}}$ ), scalar coupling ( $T_1^{\text{SC}}$ ), electric quadrupolar relaxation ( $T_1^{\text{EQ}}$ ), interactions with unpaired electrons in paramagnetic compounds, etc., which are summarized in the term:

$$\frac{1}{T_1} = \frac{1}{T_1^{\text{DD}}} + \frac{1}{T_1^{\text{CSA}}} + \frac{1}{T_1^{\text{SR}}} + \frac{1}{T_1^{\text{SC}}} + \frac{1}{T_1^{\text{EQ}}} + \frac{1}{T_1^{\text{UE}}} + \dots \quad (1.75)$$

The DD interaction is a dominant contribution to  $T_1$  relaxation and causes the most efficient relaxation of protons in molecules in solution. Nuclear spins at the excited state can transit to ground states via energy exchange with surroundings or between nuclei. The energy exchanged to the lattice may be transformed into motions of translation, rotations, and vibrations. The process of energy exchange is caused by the time-dependent fluctuation of magnetic (or electric) fields at or near the Larmor frequency. The fluctuating fields may be produced by vibrational, rotational, or translational motions of other surrounding nuclei, changes in chemical shielding, or unpaired electrons. In order for these time-dependent fluctuating fields to have significant effects on the nuclear relaxation, the random molecular motions or chemical shielding must have the same timescale as that of NMR, that is, close to the Larmor frequency. Consequently, molecular rotation and diffusion are the most efficient causes of nuclear relaxation in solution. For an aqueous solution of normal viscosity,  $T_1$  relaxation is inversely proportional to correlation time  $\tau_c$ :

$$\frac{1}{T_1} \propto \tau_c \quad (1.76)$$

It indicates that slower random motions are responsible for a shorter  $T_1$  relaxation time. Because the molecular random motions are influenced by the size of molecules, the magnitude of the correlation time is significantly dependent on the molecular weight. For small molecules with molecular weights less than 100,  $\tau_c$  is in the range of  $10^{-12}$ – $10^{-13}$  s, whereas macromolecules may have a  $\tau_c$  as large as  $10^{-8}$  s. Calculation of correlation time is a very complicated procedure in which many factors such as the shape of the molecule and different kinds of molecular motions must be taken into account. In general,  $\tau_c$  is best estimated experimentally. One of the

methods to estimate  $\tau_c$  from experimental data is to make use of the spectral density functions (section 1.10.1 and Chapter 8).

The time dependence of the process at which the initial macroscopic magnetization recovers through spin-lattice relaxation is characterized by the  $T_1$  relaxation time, which is described by the Bloch equation:

$$\frac{dM_z}{dt} = \frac{M_z - M_0}{T_1} \quad (1.77)$$

The equation describes  $T_1$  relaxation for a system without spin coupling between the nuclei. The solution for the above Bloch equation is readily obtained by integrating the equation:

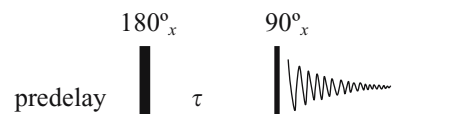
$$\frac{dM_z}{M_z - M_0} = \frac{dt}{T_1} \quad (1.78)$$

$$\int_0^{M_z} \frac{d(M_z - M_0)}{M_z - M_0} = \int_0^t \frac{dt}{T_1} \quad (1.79)$$

$$\ln M_0 - \ln(M_z - M_0) = \frac{t}{T_1} \quad (1.80)$$

$$M_z = M_0(1 - e^{-t/T_1}) \quad (1.81)$$

Because  $M_z$  is not observable directly,  $T_1$  is experimentally determined by the following pulse sequence:



A pulse sequence is a train of pulses used to manipulate the magnetization of nuclei in a static magnetic field to produce time domain signals (FID). In a pulse sequence, the  $x$  axis represents the time events, whereas the  $y$  axis describes the amplitude of the pulses. The  $180^\circ$  pulse of the  $T_1$  experiment rotates the magnetization  $M_0$  to the  $-z$  axis. Since there exists no transverse magnetization after the  $180^\circ$  pulse, the recovery of  $M_z$  comes only via  $T_1$  relaxation (along the  $z$  axis). As a result, there is no contribution from  $T_2$  transverse relaxation (Figure 1.20). After a delay  $\tau$ , a  $90^\circ$  pulse along the  $x$  axis rotates the magnetization remaining on the  $-z$  axis into the transverse plane, where it is detected. By arraying parameter  $\tau$ , the signal intensities of the resonances change from negative to positive. When  $\tau$  is set to be longer than  $T_1$ , the intensities reach maximum, which corresponds to full recovery of  $M_0$ . The  $T_1$  constant can be calculated using the intensities at different  $\tau$  values according to the following equations.

By integrating the Bloch equation for  $M_z$ , the time dependence of  $M_z$  is given by:

$$M_0 - M_z = Ae^{-t/T_1} \quad (1.82)$$

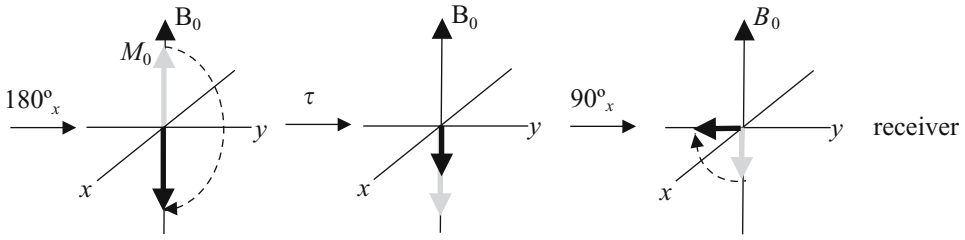


**Figure 1.20.** Vector representation of  $T_1$  relaxation time measurement.

Time parameter  $t$  is the same as the delay  $\tau$  in the inverse experiment and  $M_z$  is the transverse magnetization (signal intensity) created by the  $90^\circ$  pulse. When  $t = 0$ ,  $M_z = -M_0$ . Therefore,  $A = 2M_0$ . By substituting  $A$  with  $2M_0$  and taking logarithms on both sides of the equation, we obtain:

$$\ln(M_0 - M_z) = \ln 2M_0 - \frac{t}{T_1} \quad (1.83a)$$

$$\ln(I_0 - I) = \ln 2I_0 - \frac{t}{T_1} \quad (1.83b)$$

in which  $I$  and  $I_0$  are the peak volumes or intensities at  $t = \tau$  and at  $t = \infty$ , respectively. In practice,  $I_0$  is obtained with a  $\tau$  value long enough (30 to 60 s) to allow the magnetization to fully relax back to the equilibrium state. When  $t \equiv \tau_{\text{null}} = T_1 \ln 2$ ,  $M_z = 0$  and thus  $I_0 = 0$  ( $\tau_{\text{null}}$  is the value of the delay  $\tau$  at which  $M_z$  is zero). Therefore,  $T_1$  can be determined by:

$$T_1 = \frac{\tau_{\text{null}}}{\ln 2} = 1.443 \tau_{\text{null}} \quad (1.84)$$

$T_1$  can be calculated using Equation (1.84) for all peaks in the spectrum.

### 1.10.3. $T_2$ Relaxation

$T_2$  relaxation (also known as spin–spin or transverse relaxation) describes the decay of transverse magnetization characterized by the Bloch equation:

$$\frac{dM_x}{dt} = -\frac{M_x}{T_2} \quad (1.85)$$

or

$$\frac{dM_y}{dt} = -\frac{M_y}{T_2} \quad (1.86)$$

in which the time constant  $T_2$  is called the spin–spin or transverse relaxation time, which describes how fast transverse magnetization  $M_x$  or  $M_y$  decays to zero. Because transverse magnetizations  $M_x$  and  $M_y$  are observable signals,  $T_2$  relaxation time determines the decay rate

of an FID,  $e^{-t/T_2}$ , which corresponds to the signal line width in frequency domain,  $\Delta\nu_{1/2} = 1/\pi T_2$ , and  $\Delta\nu_{1/2}$  is defined as the line width at half height of the signal amplitude.

$T_2$  relaxation does not cause population changes in the energy states and the energy of the system is not affected by the relaxation. The process is adiabatic. In the presence of fluctuating spin–spin interactions, energy is exchanged between nuclei. During spin–spin relaxation, transition of one nucleus from a high energy state to a lower one causes another nucleus to move simultaneously from the lower state to the higher one. There is no energy exchange with the environment and hence no gain or loss in energy of the nuclear system. As a result, the phase coherence of the spins generated by the  $B_1$  field is lost.

In practice, magnetic field inhomogeneity is the dominant contribution to the transverse relaxation. Each nucleus across the sample volume experiences a slightly different  $B_0$  field caused by the inhomogeneity. Conversely, some of the chemically equivalent nuclei process faster and some slower. This results in the fanning-out of individual magnetization vectors. The net effect is a loss in phase coherence similar to that caused by fluctuating spin interactions. By taking into account the effect of  $B_0$  inhomogeneity, the transverse relaxation is described by the effective transverse relaxation time  $T_2^*$ :

$$M_y = M_0 e^{-\frac{t}{T_2^*}} \quad (1.87)$$

and

$$\Delta\nu_{1/2} = \frac{1}{\pi T_2^*} = \frac{1}{\pi T_2} + \gamma \Delta B_0 \quad (1.88)$$

Equation (1.87) tells us that  $T_2^*$  is the time when the amplitude of an FID has decayed by a factor of  $1/e$  (Figure 1.21). The first term in Equation (1.88) represents the natural line width caused by spin–spin relaxation whereas the second term is the contribution of field inhomogeneity to the spectral line width. When molecules in nonviscous liquids are moving very rapidly,  $T_1 = T_2$  for nuclei with spin  $\frac{1}{2}$ , which is called the extreme-narrowing limit. Therefore,  $T_2$  is so long that the line widths are normally narrower than 0.1 Hz.  $T_2$  can be estimated from the determined  $T_1$  relaxation time. For macromolecules or solid-state samples,  $T_1 > T_2$ , in which case the line width is broad.

When the system is not in the extreme-narrowing limit,  $T_2$  is determined experimentally by the spin echo method, which eliminates the effect of field inhomogeneity. The  $T_{1\rho}$  experiment

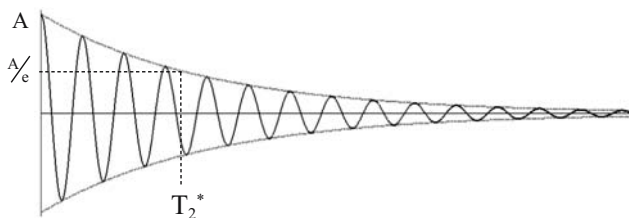


**Figure 1.21.** Effective transverse relaxation time  $T_2^*$  of an FID.



(section 8.2.2) utilizes the spin lock technique to lock the magnetization on a transverse axis, resulting in measurement of the  $T_2$  relaxation time.

For proteins and nucleic acids,  $T_2$  relaxation is dominated by the chemical shift anisotropy interaction and DD interaction with other spins (Brutscher, 2000). A single spin interaction causes autocorrelated relaxation, whereas the interference between different nuclear interactions, such as between CSA and DD or between DD and DD interactions, gives rise to cross-correlated relaxation. Both autocorrelated and cross-correlated relaxations refer to the relaxation mechanism, which differs from cross-relaxation, which refers to the relaxation pathway. In a weakly coupled two-spin- $\frac{1}{2}$  system, the contribution to  $T_2$  relaxation from the cross-correlated relaxations by CSA and DD interactions leads to different relaxation rates for individual multiplet components in the spectrum. The CSA has the same effect on the  $T_2$  relaxation of both components of the doublet. However, the influence of DD coupling on the  $T_2$  relaxation of the doublet components is antisymmetric: the effect on the  $\alpha$  transitions ( $\omega_I^{13}$  and  $\omega_S^{12}$ , Figure 1.22) is the same as for the CSA, whereas the influence

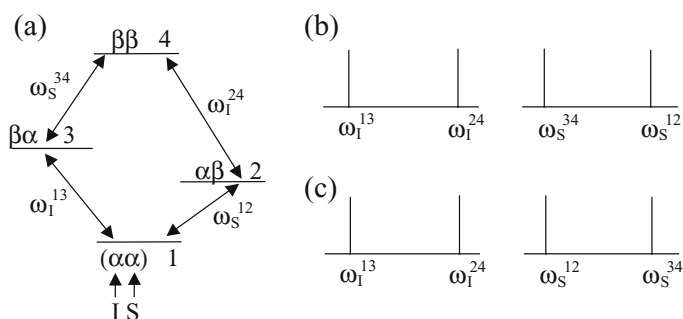


**Figure 1.22.** (a) Standard energy diagram, (b) and (c) schematic spectra of IS spin system. The doublets (c) of spin S with a negative gyromagnetic ratio are reversed relative to those with a positive gyromagnetic ratio in (b).

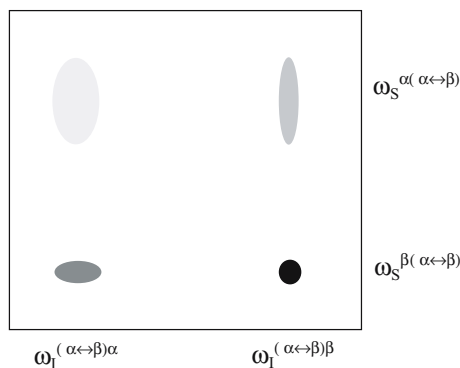


**Figure 1.23.** Schematic representation of a two-dimensional correlation spectrum of a coupled IS spin system in the presence of cross-correlated relaxation of CSA and DD coupling. The line shape of the cross peak corresponding to the two  $\beta$  transitions is not broadened by the cross-correlated relaxation due to cancellation of their opposite effects on  $T_2$  relaxation when CSA and DD coupling are aligned collinearly with comparable magnitude.

of DD coupling on the  $\beta$  transitions ( $\omega_I^{24}$  and  $\omega_S^{34}$ ) is opposite to that of CSA. When CSA and DD coupling are comparable in magnitude and the CSA principal symmetry axis is aligned collinearly to the vector of DD coupling, the line shapes of the resonances at  $\omega_I^{24}$  and  $\omega_S^{34}$  are narrowed because the effects on  $T_2$  relaxation from CSA and DD coupling cancel each other at the resonances (Figure 1.23). This property of cross-correlated relaxation has been used to reduce transverse relaxation of large proteins by TROSY experiments (Chapter 5).

### 1.11. SELECTION OF COHERENCE TRANSFER PATHWAYS

Coherence is a term representing transverse magnetization. In a coupled two-spin system, single-quantum coherence involves one spin changing its spin state ( $\alpha \rightarrow \beta$ , or  $\beta \rightarrow \alpha$ ), whereas double-quantum coherence arises from a transition in which two spins alter their states at the same time ( $\alpha\alpha \rightarrow \beta\beta$ , or  $\beta\beta \rightarrow \alpha\alpha$ ). Zero quantum coherence is referred to as a transition of  $\Delta m = 0$  with two spins changing their states in opposite directions ( $\alpha\beta \rightarrow \beta\alpha$ , or  $\beta\alpha \rightarrow \alpha\beta$ ). The transition rule governs such that only a transition with  $\Delta m = \pm 1$  between the spins is allowed, meaning that single-quantum coherence is the only directly observable coherence. The type of transition, that is, the value of  $\Delta m$ , is known as coherence order,  $p$ . A coherence order of  $p = \pm 1$  represents single-quantum coherence, whereas a coherence order of  $p = 0$  is zero-quantum coherence or  $z$  magnetization.

Because coherence order corresponds to a transition between spins, only RF pulses cause a change in coherence order from one level to another, which is referred to as coherence transfer. Delays without an RF pulse conserve the coherence orders. A diagram is used to describe the coherence transfer at the different stages of a pulse sequence, called the coherence transfer pathway (Bain, 1984; Bodenhausen *et al.*, 1984). In order to use the diagram for coherence selection, the pathway must originate at the equilibrium state in which the magnetization is along the magnetic field direction ( $z$  magnetization) possessing a coherence order of zero,  $p = 0$ . The first  $90^\circ$  pulse applied on the equilibrium  $z$  magnetization only generates single-quantum coherence,  $p = \pm 1$ , whereas the last pulse in a pulse sequence must bring the coherence to the coherence level of  $p = -1$  for the use of quadrature detection to observe the complex signals (Sørensen *et al.*, 1983). A noninitial  $90^\circ$  pulse (a  $90^\circ$  pulse other than the first one) generates higher order coherence along with single quantum coherence.

### 1.12. APPROACHES TO UNDERSTANDING NMR EXPERIMENTS

During an NMR pulse sequence, the equilibrium magnetization is manipulated to generate detectable signals. Several formalisms have been developed to describe the behavior of nuclear magnetization during a pulse sequence. In this section, three theoretical treatments (vector model, product operator formalism, and density matrix) used to describe how magnetization is transferred during NMR experiments are briefly discussed. Simple pulse sequences are used as examples to help understand the approaches.

Questions to be addressed include:

1. What are the advantages and limitations of each approach?
2. How are the approaches used to describe how experiments work?

### 1.12.1. Vector Model

For a variety of experiments [such as the one-pulse experiment (Figure 1.7),  $T_1$  measurement, spin echoes, polarization transfer experiments, and composite pulses] the vector model remains a useful approach for analysis of the experiments because of its visualization and simplicity. However, the vector model is inadequate to analyze certain experiments such as DEPT (distortionless enhancement by polarization transfer, Doddrell *et al.*, 1982; Bendall and Pegg, 1983) because it is unable to describe multiple quantum coherence.

Shown in Figure 1.24 is the vector representation of magnetization during the pulse sequence of INEPT (insensitive nuclei enhanced by polarization transfer, Morris and Freeman, 1979), which is used to transfer magnetization from one nucleus (usually  $^1\text{H}$ ) to a heteronucleus through  $J$  coupling. It is the most utilized building block of many heteronuclear NMR pulse sequences. The first  $90^\circ$   $^1\text{H}$  pulse rotates the  $^1\text{H}$  magnetization onto the  $y$  axis at point a. After the first  $1/(4J_{\text{CH}})$  delay, each of the doublets caused by the  $J_{\text{CH}}$  coupling is  $45^\circ$  away from the  $y$  axis. The simultaneous  $180^\circ$  pulses on both  $^1\text{H}$  and  $^{13}\text{C}$  refocus the chemical shift but allow the coupled  $^1\text{H}$  vectors to continue to diverge. This can be understood by considering the effect of  $^1\text{H}$  and  $^{13}\text{C}$   $180^\circ$  pulses individually. After the  $^1\text{H}$   $180^\circ$  pulse flips the doublets about the  $x$  axis, the  $^{13}\text{C}$   $180^\circ$  inverts the population of  $^{13}\text{C}$  states of the coupled doublets but has no effect on uncoupled chemical shift. Consequently, the magnetization in the  $^{13}\text{C}$   $\alpha$  state becomes that in the  $\beta$  state, and vice versa. It is represented in the vector diagram at point c that the slower and faster vectors exchange places, resulting in the vectors rotating in the other direction (c). After the second  $1/(4J_{\text{CH}})$  delay, the two vectors are  $180^\circ$  out of phase and aligned on the  $x$  axis (d). The following  $^1\text{H}$   $90^\circ$  pulse rotates the  $^1\text{H}$  magnetization components back

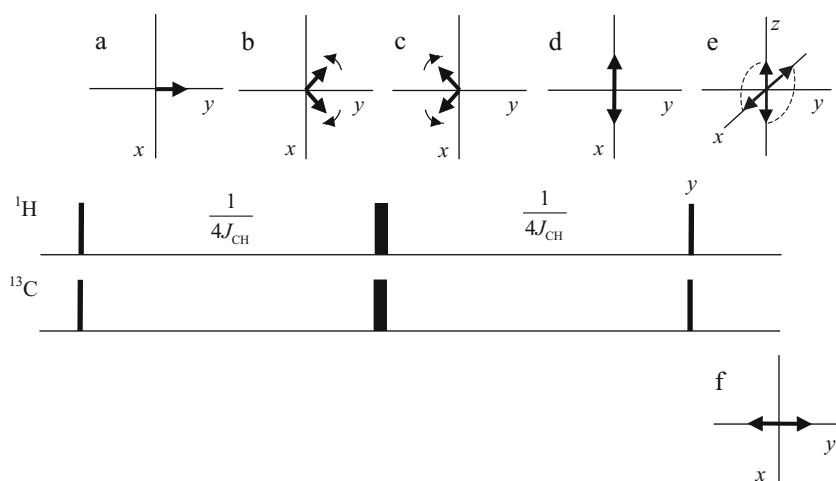


**Figure 1.24.** Vector representation of an INEPT experiment. The narrow and wide bars are  $90^\circ$  and  $180^\circ$  pulses, respectively. All pulses are  $x$  phase except the last  $^1\text{H}$   $90^\circ_y$ . After a  $90^\circ_x$  pulse (point a), the  $^1\text{H}$  magnetization is on the  $y$  axis. During the delay period of  $1/(4J_{\text{CH}})$ , the two coupled spins process with different frequencies in the rotating frame: one is slower than the rotating frame frequency and the other faster, assuming that the carrier frequency (rotating frame frequency) is set to the center of the  $J$  coupled peaks.

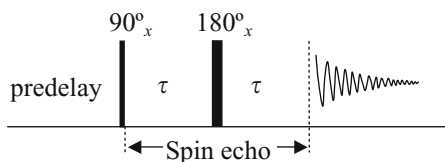
to the  $z$  and  $-z$  axes (e), and the  $^{13}\text{C}$   $90^\circ$  pulse brings the coupled magnetization components back to the  $xy$  plane, which results in detectable anti-phase magnetization (f).

### 1.12.2. Product Operator Description of Building Blocks in a Pulse Sequence

Product operator formalism has become a popular approach for the theoretical description of NMR experiments because it combines the simplicity and visualization of vector representation with quantum mechanics. The approach utilizes a linear combination of base operators to express the density matrix. Shorthand notation can be used to describe the operator matrices (Sørensen *et al.*, 1983). Therefore, it does not require an understanding of quantum mechanics to utilize the formalism. The standard notation of the product operators for a two-spin system with their physical interpretation is explained in Appendix A.

#### 1.12.2.1. Spin-Echo of Uncoupled Spins

The spin echo experiment consists of two delays separated by a  $180^\circ$  pulse after the transverse magnetization is produced (Carr and Purcell, 1954):



For an isolated spin, the magnetization starting at the equilibrium state proportional to  $I_z$  will undergo a series of changes during the spin echo sequence. Upon the application of the first  $90^\circ_x$  pulse [denoted by  $(\pi/2)I_x$ ], the equilibrium magnetization  $I_z$  is converted to  $-I_y$ :

$$I_z \xrightarrow{(\pi/2)I_x} -I_y \quad (1.89)$$

During the first period  $\tau$  of free precession of the spin echo, the magnetization evolves to:

$$-I_y \xrightarrow{\Omega_i I_z \tau} -I_y \cos(\Omega_i \tau) + I_x \sin(\Omega_i \tau) \quad (1.90)$$

The  $180^\circ_x$  pulse inverts  $I_y$  magnetization, but does not have any effect on  $I_x$  magnetization:

$$-I_y \cos(\Omega_i \tau) + I_x \sin(\Omega_i \tau) \xrightarrow{\pi I_x} I_y \cos(\Omega_i \tau) + I_x \sin(\Omega_i \tau) \quad (1.91)$$

In the final delay of the spin echo sequence, the free precession yields

$$\begin{aligned} I_y \cos(\Omega_i \tau) + I_x \sin(\Omega_i \tau) &\xrightarrow{\Omega_i I_z \tau} [I_y \cos^2(\Omega_i \tau) - I_x \sin(\Omega_i \tau) \cos(\Omega_i \tau)] \\ &\quad + [I_x \sin(\Omega_i \tau) \cos(\Omega_i \tau) + I_y \sin^2(\Omega_i \tau)] \end{aligned} \quad (1.92)$$

Because  $\cos^2 \theta + \sin^2 \theta = 1$ , Equation (1.92) reduces to

$$I_y \cos(\Omega_i \tau) + I_x \sin(\Omega_i \tau) \xrightarrow{\Omega_i I_z \tau} I_y \quad (1.93)$$

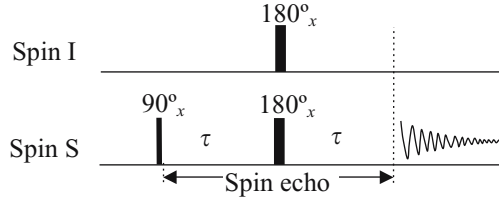
Therefore, the net effect of a spin echo sequence on uncoupled spins is to change the sign of the transverse magnetization:

$$-I_y \xrightarrow{\tau \rightarrow \pi I_x \rightarrow \tau} I_y \quad (1.94)$$

There is no net evolution of the chemical shift during the spin echo sequence because evolution of the chemical shift is refocused upon completion of the spin echo sequence.

#### 1.12.2.2. Spin-Echo of Coupled Spins

For two coupled spins, the spin-echo sequence can be applied to homonuclear spins or the following pulse sequence can be used for coupled heteronuclear spins:



The two  $180^\circ$  pulses on the heteronuclear spins will have the same effect as a nonselective homonuclear  $180^\circ$  pulse on the coupled homonuclear spins. During the evolution period, scalar coupling is the only interaction to be considered because evolution under the chemical shift interaction will be refocused by the spin echo sequence as described for the uncoupled spin. For heteronuclear magnetization after a  $90^\circ_x$  pulse on the S spin, the evolution during the first  $\tau$  period under the scalar coupling  $J_{IS}$  converts the in-phase magnetization of  $-S_y$  to orthogonal anti-phase magnetization, which is represented by the product operators:

$$-S_y \xrightarrow{\pi J_{IS} \tau} -S_y \cos(\pi J_{IS} \tau) + 2I_z S_x \sin(\pi J_{IS} \tau) \quad (1.95)$$

A  $180^\circ$  pulse on the S spin does not have any effect on the I spin and vice versa. Therefore, the  $180^\circ$  pulse on S spin changes the sign of  $S_y$  whereas the  $180^\circ$  pulse on the I spin inverts  $I_z$ :

$$\begin{aligned} -S_y \cos(\pi J_{IS} \tau) + 2I_z S_x \sin(\pi J_{IS} \tau) &\xrightarrow{\pi S_x} S_y \cos(\pi J_{IS} \tau) + 2I_z S_x \sin(\pi J_{IS} \tau) \\ &\xrightarrow{\pi I_x} S_y \cos(\pi J_{IS} \tau) - 2I_z S_x \sin(\pi J_{IS} \tau) \end{aligned} \quad (1.96)$$

The conversion of the magnetization during the second evolution is described by:

$$\begin{aligned} S_y \cos(\pi J_{IS} \tau) - 2I_z S_x \sin(\pi J_{IS} \tau) &\xrightarrow{\pi J_{IS} \tau} [S_y \cos^2(\pi J_{IS} \tau) - 2I_z S_x \cos(\pi J_{IS} \tau) \sin(\pi J_{IS} \tau)] \\ &+ [-2I_z S_x \sin(\pi J_{IS} \tau) \cos(\pi J_{IS} \tau) - S_y \sin^2(\pi J_{IS} \tau)] \end{aligned} \quad (1.97)$$

Using  $\cos^2 \theta - \sin^2 \theta = \cos 2\theta$  and  $2 \cos \theta \sin \theta = \sin 2\theta$ , the equation is simplified to:

$$S_y \cos(\pi J_{IS} \tau) - 2I_z S_x \sin(\pi J_{IS} \tau) \xrightarrow{\pi J_{IS} \tau} S_y \cos(2\pi J_{IS} \tau) - 2I_z S_x \sin(2\pi J_{IS} \tau) \quad (1.98)$$

Therefore,

$$-S_y \xrightarrow{\tau \rightarrow \pi(I_x + S_x) \rightarrow \tau} S_y \cos(2\pi J_{IS} \tau) - 2I_z S_x \sin(2\pi J_{IS} \tau) \quad (1.99)$$

If  $\tau$  is set to  $1/(2J_{IS})$ , then

$$-S_y \xrightarrow{\tau \rightarrow \pi(I_x + S_x) \rightarrow \tau} S_y \quad (1.100)$$

which gives inverted in-phase magnetization. When  $\tau$  is set to  $1/(4J_{IS})$ , anti-phase coherence is generated:

$$-S_y \xrightarrow{\tau \rightarrow \pi(I_x + S_x) \rightarrow \tau} -2I_z S_x \quad (1.101)$$

For initial magnetization from spin I,  $-I_y$ , the result can be obtained by interchanging the I and S operators in the equations for the magnetization initiated at  $-S_y$ :

$$-I_y \xrightarrow{\tau \rightarrow \pi(I_x + S_x) \rightarrow \tau} -2I_x S_z \quad (1.102)$$

The above result is for the real part of the FID. If considering the complex data observed by quadrature detection, the operator of  $I_x$  in Equation (1.101) or (1.102) is replaced by raising operator  $I^+$  and lowering operator  $I^-$

$$I^+ = I_x + iI_y \quad (1.103)$$

$$I^- = I_x - iI_y$$

in which  $I_y$  is the observable imaginary magnetization.

#### 1.12.2.3. *Insensitive Nuclei Enhanced by Polarization Transfer*

The pulse sequence (Figure 1.24) in INEPT before the final two  $90^\circ$  pulses is the same as the heteronuclear echo sequence. Hence, the anti-phase magnetization of  $-2I_x S_z$  is generated when  $\tau = 1/(4J_{IS})$ . In the next step of INEPT, a  $90_y^\circ$  pulse is applied to spin I and a  $90_x^\circ$  pulse to spin S simultaneously, which produces an anti-phase observable S magnetization given by:

$$-2I_x S_z \xrightarrow{(\pi/2)(I_y + S_x)} -2I_z S_y \quad (1.104)$$

or

$$-I_y \xrightarrow{\text{INEPT}} -2I_z S_y$$

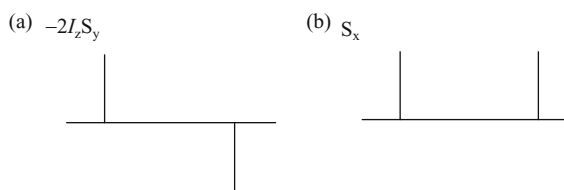


**Figure 1.25.** The doublets of spin S corresponding to the product operator of (a) anti-phase and (b) in-phase coherence.

The sensitivity of spin S in the INEPT is enhanced by spin I for a factor of  $\gamma_I/\gamma_S$ . In the anti-phase signal, one component of the doublet has negative intensity, whereas the other is positive. The INEPT sequence is used in multidimensional heteronuclear experiments to transfer magnetization through scalar coupling between heteronuclei.

Because of the anti-phase character of the magnetization after INEPT,  $^1\text{H}$  decoupling, which is used to increase sensitivity, cannot be applied during acquisition. A refocused INEPT sequence is used to convert anti-phase magnetization in the INEPT sequence into in-phase coherence by appending an additional echo sequence after the INEPT:

$$\begin{aligned}
 -2I_z S_y &\xrightarrow{\pi J_{IS}\tau} -2I_z S_y \cos(\pi J_{IS}\tau) + S_x \sin(\pi J_{IS}\tau) \\
 &\xrightarrow{\pi(I_x + S_x)} -2I_z S_y \cos(\pi J_{IS}\tau) + S_x \sin(\pi J_{IS}\tau) \\
 &\xrightarrow{\pi J_{IS}\tau} -2I_z S_y \cos(2\pi J_{IS}\tau) + S_x \sin(2\pi J_{IS}\tau)
 \end{aligned} \quad (1.105)$$

When  $\tau = 1/(4J_{IS})$ , the cosine term equals zero. Hence, the magnetization after the last echo sequence is given by:

$$-2I_z S_y \xrightarrow{\tau \rightarrow \pi(I_x + S_x) \rightarrow \tau} S_x \quad (1.106)$$

which is an observable in-phase magnetization. Therefore, for the refocused INEPT, decoupling can be applied during acquisition to increase sensitivity by collapsing the  $I$ - $S$  coupling doublet [Figure 1.25(b)].

### 1.12.3. Introduction to Density Matrix

The density matrix approach (Fano, 1957; Howarth *et al.*, 1986; Hore *et al.*, 2001) is used to treat a more complicated case involving two or more spins by solving density matrices for the operators involved in NMR experiments. For a system consisting of uncoupled spins of  $\frac{1}{2}$ , the energy  $E$  of the two states for the Schrödinger equation is given by:

$$\mathbf{H}(t)\Psi(t) = E\Psi(t) \quad (1.107)$$

The equation describes how the time-dependent Hamiltonian operator  $\mathbf{H}(t)$  governs the time dependence of the system wave function  $\Psi(t)$ . The system wave function can be represented

in Dirac notation (Dirac, 1967) by a linear combination of the basis functions  $\phi_1 = |\alpha\rangle$  and  $\phi_2 = |\beta\rangle$  for a single spin  $\frac{1}{2}$  system:

$$\Psi(t) = C_1|\alpha\rangle + C_2|\beta\rangle \quad (1.108)$$

$$\mathbf{H} = -\gamma B_0 \hbar \hat{\mathbf{I}}_z = \hbar \omega_0 \hat{\mathbf{I}}_z \quad (1.109)$$

in which  $\omega_0 = -\gamma B_0$  is the Larmor frequency, and

$$\mathbf{H}|\alpha\rangle = \frac{1}{2}|\alpha\rangle, \quad \mathbf{H}|\beta\rangle = -\frac{1}{2}|\beta\rangle \quad (1.110)$$

in which the eigenvalues are represented in units of  $\hbar \omega_0$  for simplicity. Populations of the energy states are given by:

$$N_\alpha = \frac{e^{(-E_1/kT)}}{\sum_{i=1}^2 e^{(-E_i/kT)}} = \frac{1}{2} - \frac{E_1}{2kT} = \frac{1}{2} \left( 1 - \frac{\hbar \omega_0}{2kT} \right) \quad (1.111)$$

$$N_\beta = \frac{e^{(-E_2/kT)}}{\sum_{i=1}^2 e^{(-E_i/kT)}} = \frac{1}{2} - \frac{E_2}{2kT} = \frac{1}{2} \left( 1 + \frac{\hbar \omega_0}{2kT} \right) \quad (1.112)$$

The eigenvalues (energy) can be used to represent the operator  $\hat{\mathbf{I}}_z$  in terms of a matrix:

$$\mathbf{I}_z = \begin{pmatrix} \frac{1}{2} & 0 \\ 0 & -\frac{1}{2} \end{pmatrix} \quad (1.113)$$

The operators of the transverse  $x$  and  $y$  components interconvert  $|\alpha\rangle$  and  $|\beta\rangle$  because  $|\alpha\rangle$  and  $|\beta\rangle$  are not the eigenstates of the operators:

$$\hat{\mathbf{I}}_x|\alpha\rangle = \frac{1}{2}|\beta\rangle, \quad \hat{\mathbf{I}}_x|\beta\rangle = \frac{1}{2}|\alpha\rangle \quad (1.114)$$

$$\hat{\mathbf{I}}_y|\alpha\rangle = \frac{1}{2}i|\beta\rangle, \quad \hat{\mathbf{I}}_y|\beta\rangle = -\frac{1}{2}i|\alpha\rangle \quad (1.115)$$

which can be understood by the raise and lower operators  $\hat{\mathbf{I}}_+$  and  $\hat{\mathbf{I}}_-$ :

$$\hat{\mathbf{I}}_x|\alpha\rangle = \frac{1}{2}(\hat{\mathbf{I}}_+ + \hat{\mathbf{I}}_-)|\alpha\rangle = \frac{1}{2}(0 + |\beta\rangle) = \frac{1}{2}|\beta\rangle \quad (1.116)$$

$$\hat{\mathbf{I}}_y|\beta\rangle = \frac{i}{2}(\hat{\mathbf{I}}_- - \hat{\mathbf{I}}_+)|\beta\rangle = \frac{i}{2}(0 - |\alpha\rangle) = -\frac{i}{2}|\alpha\rangle \quad (1.117)$$

The corresponding matrices for the operators are given by:

$$\mathbf{I}_x = \begin{pmatrix} 0 & \frac{1}{2} \\ \frac{1}{2} & 0 \end{pmatrix} = \frac{1}{2} \begin{pmatrix} 0 & 1 \\ 1 & 0 \end{pmatrix} = \frac{1}{2} \boldsymbol{\sigma}_x \quad (1.118)$$

$$\mathbf{I}_y = \begin{pmatrix} 0 & -\frac{1}{2}i \\ \frac{1}{2}i & 0 \end{pmatrix} = \frac{1}{2} \begin{pmatrix} 0 & -i \\ i & 0 \end{pmatrix} = \frac{1}{2} \boldsymbol{\sigma}_y \quad (1.119)$$



in which  $\sigma_x$ ,  $\sigma_y$ , and  $\sigma_z$  are the Pauli matrices with the property of  $\sigma_r^2 = \sigma_0$  for  $r = x, y, z$ :

$$\sigma_z = \begin{pmatrix} 1 & 0 \\ 0 & -1 \end{pmatrix} \quad (1.120)$$

$$\sigma_0 = \begin{pmatrix} 1 & 0 \\ 0 & 1 \end{pmatrix} \quad (1.121)$$

The bras and kets are represented by vectors:

$$\langle \alpha | = (1 \quad 0); \quad \langle \beta | = (0 \quad 1) \quad (1.122)$$

$$| \alpha \rangle = \begin{pmatrix} 1 \\ 0 \end{pmatrix}; \quad | \beta \rangle = \begin{pmatrix} 0 \\ 1 \end{pmatrix} \quad (1.123)$$

By combining the matrices  $\mathbf{I}_x$  and  $\mathbf{I}_y$  the matrices for the raise and lower operators can be obtained:

$$\mathbf{I}_+ = \mathbf{I}_x + i\mathbf{I}_y = \begin{pmatrix} 0 & 1 \\ 0 & 0 \end{pmatrix} \quad (1.124)$$

$$\mathbf{I}_- = \mathbf{I}_x - i\mathbf{I}_y = \begin{pmatrix} 0 & 0 \\ 1 & 0 \end{pmatrix} \quad (1.125)$$

Matrices  $\mathbf{I}_x$ ,  $\mathbf{I}_y$ , and  $\mathbf{I}_z$  represent the magnetization along the  $x$ ,  $y$ , and  $z$  axes, respectively. Quantum mechanics states that the expectation value of an operator  $\hat{A}$  depends on the products of coefficients, which is given by:

$$\langle \hat{A} \rangle = \langle \Psi(t) | \hat{A} | \Psi(t) \rangle = \sum_{k,l} C_k^* C_l \langle k | \hat{A} | l \rangle = \sum_{k,l} C_k^* C_l A_{kl} \quad (1.126)$$

in which  $C_k$ ,  $C_l$  are defined in Equation (1.108) for a single spin  $\frac{1}{2}$  system. Therefore, it is useful to define a density matrix  $\rho(t)$  with an individual matrix element in the term of:

$$\rho_{lk} = \langle k | \rho | l \rangle = C_k^* C_l \quad (1.127)$$

The density matrix for a single spin  $\frac{1}{2}$  system at equilibrium state is given by

$$\rho = \begin{pmatrix} \rho_{11} & \rho_{12} \\ \rho_{21} & \rho_{22} \end{pmatrix} = \begin{pmatrix} N_\alpha & 0 \\ 0 & N_\beta \end{pmatrix} = \frac{1}{2} \begin{pmatrix} 1 & 0 \\ 0 & 1 \end{pmatrix} + \frac{1}{2} \begin{pmatrix} \delta & 0 \\ 0 & -\delta \end{pmatrix} = \frac{1}{2} \sigma_0 + \delta \mathbf{I}_z \quad (1.128)$$

in which  $\delta = -\hbar\omega_0/2kT$ . The unit matrix  $\sigma_0$  is not of NMR interest because it does not evolve during any Hamiltonian. The  $\delta$  is a scaling factor. Thus  $\sigma_0$  and  $\delta$  are often omitted.

The expectation value of  $\hat{A}$  is thus represented by the trace of the product  $\rho$  and  $A$ :

$$\langle \hat{A} \rangle = \sum_{k,l} C_k^* C_l A_{kl} = \sum_{k,l} \rho_{lk} A_{kl} = \sum_l (\rho \mathbf{A})_{ll} = \text{Tr}(\rho \mathbf{A}) \quad (1.129)$$

$\text{Tr}()$  is the trace of a matrix defined as the sum of the diagonal elements of the matrix (here, the product of the matrices). By solving the Liouville-von Neumann equation

$$i \frac{d\hat{\rho}}{dt} = [\mathbf{H}, \hat{\rho}] \quad (1.130)$$

the time-dependent density matrix can be described in terms of operator exponentials:

$$\rho(t) = e^{-i\mathbf{H}t} \rho(0) e^{i\mathbf{H}t} \quad (1.131)$$

For RF pulses in the rotating frame, the Hamiltonian is given by:

$$\mathbf{H} = \omega_1 \hat{\mathbf{I}}_x \quad \text{or} \quad \mathbf{H} = \omega_1 \hat{\mathbf{I}}_y \quad (1.132)$$

The matrices for the Hamiltonian of  $x$  and  $y$  pulses and free precession can be obtained by using expansion of the exponential:

$$e^{\pm iaA} = \sigma_0 \cos a \pm i\mathbf{A} \sin a \quad (1.133)$$

$$e^{\pm i\phi \hat{\mathbf{I}}_x} = \sigma_0 \cos \frac{\phi}{2} \pm i2\mathbf{I}_x \sin \frac{\phi}{2} = \begin{pmatrix} \cos \frac{\phi}{2} & \pm i \sin \frac{\phi}{2} \\ \pm i \sin \frac{\phi}{2} & \cos \frac{\phi}{2} \end{pmatrix} \xrightarrow{\phi=\pi/2} \frac{1}{\sqrt{2}} \begin{pmatrix} 1 & \pm i \\ \pm i & 1 \end{pmatrix} \quad (1.134)$$

$$e^{\pm i\phi \hat{\mathbf{I}}_y} = \begin{pmatrix} \cos \frac{\phi}{2} & \pm \sin \frac{\phi}{2} \\ \mp \sin \frac{\phi}{2} & \cos \frac{\phi}{2} \end{pmatrix} \xrightarrow{\phi=\pi/2} \frac{1}{\sqrt{2}} \begin{pmatrix} 1 & \pm 1 \\ \mp 1 & 1 \end{pmatrix} \quad (1.135)$$

$$e^{\pm i\omega t \hat{\mathbf{I}}_z} = \begin{pmatrix} e^{\pm i\omega t/2} & 0 \\ 0 & e^{\mp i\omega t/2} \end{pmatrix} \quad (1.136)$$

in which  $\phi = \omega_1 t$  is the pulse angle rotated by the RF field with strength  $B_1 = \hbar\omega_1$ , and  $\omega$  is the resonance frequency of the spin in the rotating frame. When on-resonance,  $\omega = 0$ . For a one-pulse experiment with a  $90^\circ_x$  pulse applied to the initial magnetization  $I_z$ , the density matrix after the  $90^\circ$  pulse is given by:

$$\rho(t) = e^{-i(\pi/2)\hat{\mathbf{I}}_x} \rho(0) e^{i(\pi/2)\hat{\mathbf{I}}_x} \quad (1.137)$$

$$= e^{-i(\pi/2)\hat{\mathbf{I}}_x} \mathbf{I}_z e^{i(\pi/2)\hat{\mathbf{I}}_x} = \frac{1}{2} \begin{pmatrix} 0 & i \\ -i & 0 \end{pmatrix} = -\mathbf{I}_y \quad (1.138)$$

We now define a transform matrix as:

$$\mathbf{U}_H \rho(0) = e^{-iHt} \rho(0) e^{iHt} \quad (1.139)$$

$$\rho(t) = \mathbf{U}_{\frac{\pi}{2}x} \mathbf{I}_z = e^{-i\frac{\pi}{2}\hat{\mathbf{I}}_x} \mathbf{I}_z e^{i\frac{\pi}{2}\hat{\mathbf{I}}_x} = -\mathbf{I}_y \quad (1.140)$$

The above equation for  $\rho(t)$  is equivalent to the product operator representation of:

$$\mathbf{I}_z \xrightarrow{(\pi/2)\mathbf{I}_x} -\mathbf{I}_y \quad (1.141)$$

The density matrix for the observed magnetization changing with time is given by:

$$\begin{aligned} \rho(t) = \mathbf{U}_{H_R}(-\mathbf{I}_y) &= \frac{1}{2} \begin{pmatrix} e^{-i\omega t/2} & 0 \\ 0 & e^{i\omega t/2} \end{pmatrix} \begin{pmatrix} 0 & i \\ -i & 0 \end{pmatrix} \begin{pmatrix} e^{i\omega t/2} & 0 \\ 0 & e^{-i\omega t/2} \end{pmatrix} \\ &= \frac{1}{2} \begin{pmatrix} 0 & ie^{-i\omega t} \\ -ie^{i\omega t} & 0 \end{pmatrix} \end{aligned} \quad (1.142)$$

The observable magnetization is obtained by the trace of the product of the density matrix with the raise operator:

$$\overline{M(t)} = \text{Tr}(\rho(t)\mathbf{I}_+) = -\frac{1}{2}ie^{i\omega t} = \frac{1}{2}(\sin \omega t - i \cos \omega t) \quad (1.143)$$

By now we have seen all of the basic concepts necessary to predict the behavior of an isolated spin system in the absence of relaxation.

## QUESTIONS

- 1.1. In an inversion-recovery experiment, signal A has zero intensity when  $\tau = 380$  ms. Estimate the spin-lattice relaxation time  $T_1$  for the signal.
- 1.2. Assuming that a signal has an intensity of 100 observed using a  $90^\circ$  pulse, what is the intensity of the signal if a  $45^\circ$  pulse is used?
- 1.3. What is the longest dwell time one could use to collect  $^1\text{H}$  data for a spectrum with 10 ppm on a 600 MHz spectrometer and the carrier frequency in the center of the spectrum?
- 1.4. What is the frequency of  $^{13}\text{C}$  in the laboratory frame on a 500 MHz instrument? And what is its frequency in the rotating frame (on resonance)?
- 1.5. Assuming that we have a 100%  $^{13}\text{C}$  enriched sample and we have obtained  $^1\text{H}$  and  $^{13}\text{C}$  spectra with one transient, what is the intensity of  $^{13}\text{C}$  likely to be relative to the  $^1\text{H}$  spectrum?

- 1.6. Assuming that the DSS signal has a resonance frequency of 600.0123456 MHz, what is the reference frequency for  $^{13}\text{C}$  and  $^{15}\text{N}$  if  $^{13}\text{C}$  and  $^{15}\text{N}$  are chosen according to the ratio of their gyromagnetic ratios to that of  $^1\text{H}$  (listed in Table 1.1)?
- 1.7. What is the frequency for 170 ppm and 58 ppm of  $^{13}\text{C}$ , and for 118 ppm of  $^{15}\text{N}$  using the reference frequencies in question 1.6?
- 1.8. Assuming that the  $^3J_{\text{HNH}\alpha}$  coupling constant of a residue in a protein is about 10 Hz, what is likely the value of torsion angle  $\phi$ ?
- 1.9. Where is the magnetization after applying a spin echo pulse sequence  $90^\circ_x - \tau - 180^\circ_x - \tau$ ?
- 1.10. When is a high power rectangular RF pulse used? What three parameters are needed to be specified?

## APPENDIX A: PRODUCT OPERATORS

### A1. Uncoupled Spins

For an uncoupled spin system, the product operators can be applied to individual spins. For a spin- $\frac{1}{2}$  nucleus, there are three basic operators used to describe the spin magnetization during NMR experiments,  $I_x$ ,  $I_y$ , and  $I_z$ , which are the  $x$ ,  $y$ , and  $z$  components of spin  $I$  magnetization. The transformations of these operators after a  $90^\circ(\pi/2)$  pulse are given by:

$$\begin{array}{ll}
 I_x \xrightarrow{(\pi/2)I_x} I_x & I_x \xrightarrow{(\pi/2)I_y} -I_z \\
 I_y \xrightarrow{(\pi/2)I_x} I_z & I_y \xrightarrow{(\pi/2)I_y} I_y \\
 I_z \xrightarrow{(\pi/2)I_x} -I_y & I_z \xrightarrow{(\pi/2)I_y} I_x
 \end{array} \tag{A1.1}$$

in which  $(\pi/2)I_x$  and  $(\pi/2)I_y$  are the  $90^\circ$  pulses applied along the  $x$  and  $y$  axes, respectively. For a free precession during time  $t$  at resonance  $\Omega$ , the transformations of the three operators are given by:

$$I_x \xrightarrow{\Omega t} I_x \cos \Omega t + I_y \sin \Omega t \tag{A1.2}$$

$$I_y \xrightarrow{\Omega t} I_y \cos \Omega t - I_x \sin \Omega t \tag{A1.3}$$

$$I_z \xrightarrow{\Omega t} I_z \tag{A1.4}$$

The sign of the above rotations are shown in Figure A1.1. An example of applying the product operators to describe the spin echo experiment of uncouple spins is discussed in section 1.12.2.1.

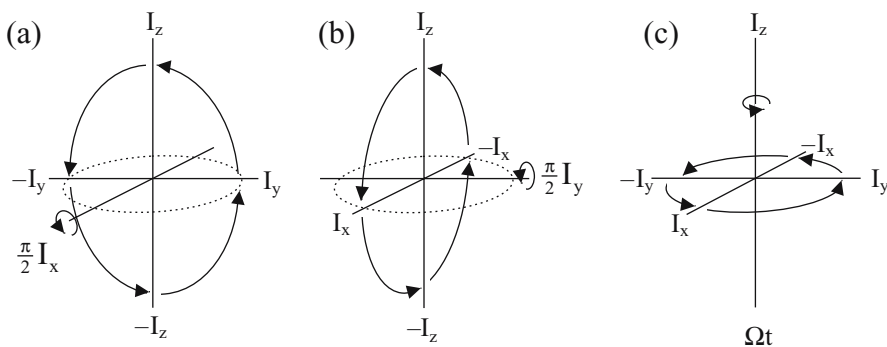


**Figure A1.1.** The transformations of the product operators for uncoupled spin I (a) after a  $90^\circ_x$  pulse, (b) after a  $90^\circ_y$  pulse and (c) during free precession  $\Omega t$ . (Ziessow, D., *Concept Magn. Reson.* **2**, 81 (1990); Hore *et al.* *NMR: The Toolkit*, Oxford University Press, Oxford (2001).)

**TABLE A1.1**  
Product Operators for a Coupled  
Two-Spin IS System

	$S_x$	$S_y$	$S_z$
<b><math>I_x</math></b>	$2I_x S_x$	$2I_x S_y$	$2I_x S_z$
<b><math>I_y</math></b>	$2I_y S_x$	$2I_y S_y$	$2I_y S_z$
<b><math>I_z</math></b>	$2I_z S_x$	$2I_z S_y$	$2I_z S_z$

*Note:* The product operators in bold are the in-phase magnetization, the four product operators ( $2I_x S_x$ ,  $2I_x S_y$ ,  $2I_y S_x$  and  $2I_y S_y$ ) are the multiple-quantum coherences, and the rest are the anti-phase magnetization.

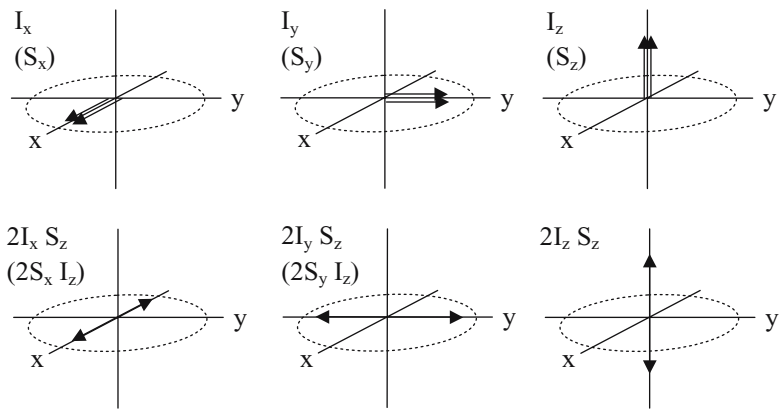


**Figure A1.2.** Vector representation of product operators for in-phase and anti-phase magnetization for spin I (or spin S) in a coupled two-spin system.

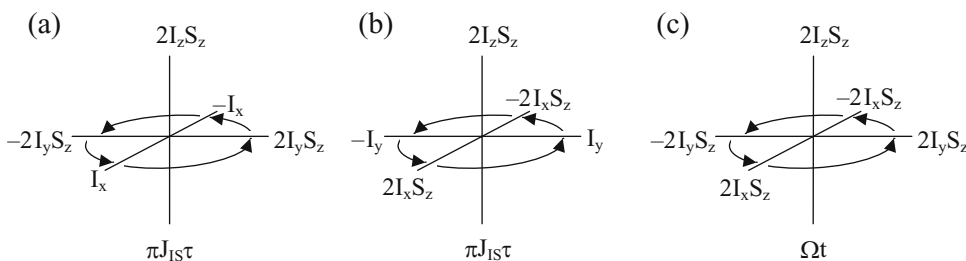


**Figure A1.3.** The transformations of the product operators for a two coupled spin IS system by scalar coupling  $J_{IS}$  (a) and (b) during evolution under the influence of  $J_{IS}$  coupling for a period  $\tau$ , and (c) during free precession  $\Omega t$ .

## A2. Two Coupled Spins

The spin system of two coupled spins I and S may be either homonuclear or heteronuclear spin systems. For a homonuclear spin system, nonselective RF pulses act on both spins, whereas the RF pulses rotate only the specific spin because the Larmor frequencies of the heteronuclei are several tens of megahertz off-resonance to each other. In addition to the six operators for the  $x$ ,  $y$ , and  $z$  components of individual spin (i.e.,  $I_x$ ,  $I_y$ , and  $I_z$  for spin I, and  $S_x$ ,  $S_y$ , and  $S_z$  for spin S), nine product operators represent the coupling between the two spins, which are summarized in Table A1.1, of which five product operators for the anti-phase magnetization are illustrated in Figure A1.2 in vector representation. The transformations of the product operators during evolution under the influence of  $J_{IS}$  coupling for a period  $\tau$  are given by:

$$I_x \xrightarrow{\pi J_{IS}\tau} I_x \cos \pi J_{IS}\tau + 2I_y S_z \sin \pi J_{IS}\tau \quad (\text{A1.5})$$

$$I_y \xrightarrow{\pi J_{IS}\tau} I_y \cos \pi J_{IS}\tau - 2I_x S_z \sin \pi J_{IS}\tau \quad (\text{A1.6})$$

$$I_z \xrightarrow{\pi J_{IS}\tau} I_z \quad (\text{A1.7})$$

$$2I_x S_z \xrightarrow{\pi J_{IS}\tau} 2I_x S_z \cos \pi J_{IS}\tau + I_y \sin \pi J_{IS}\tau \quad (\text{A1.8})$$

$$2I_y S_z \xrightarrow{\pi J_{IS}\tau} 2I_y S_z \cos \pi J_{IS}\tau - I_x \sin \pi J_{IS}\tau \quad (\text{A1.9})$$

$$2I_z S_z \xrightarrow{\pi J_{IS}\tau} 2I_z S_z \quad (\text{A1.10})$$

The product operators for spin S can be obtained similarly by interchanging I and S in Equations A1.5–A1.10. The above rules for the transformations of product operators are summarized in Figure A1.3.

## REFERENCES

- Abragam, A., *Principles of Nuclear Magnetism*, Clarendon Press, Oxford (1961).  
 Baber, J.L., D. Libutti, D. Levens, and N. Tjandra, *J. Mol. Biol.* **289**, 949 (1999).

- Bain, A.D., *J. Magn. Reson.* **56**, 418 (1984).
- Barkhuysen, H., R. De Beer, W.M.M.J. Bovee, and D. VanOrmondt, *J. Magn. Reson.* **61**, 465 (1985).
- Bax, A., G. Kontaxis, and N. Tjandra, *Meth. Enzymol.* **339**, 127 (2001).
- Bendall, M.R. and D.T. Pegg, *J. Magn. Reson.* **53**, 272 (1983).
- Bloch, F., *Phys. Rev.* **70**, 460 (1946).
- Bodenhausen, G., H. Kogler, and R.R. Ernst, *J. Magn. Reson.* **58**, 370 (1984).
- Bracewell, R.N., *The Fourier Transformation and its Application*, McGraw-Hill, New York (1986).
- Brutscher, B., *Concepts Magn. Reson.* **12**, 207 (2000).
- Carr, H. Y. and E. M. Purcell, *Phys. Rev.* **94**, 630 (1954).
- de Alba, E. and N. Tjandra, *Prog. Nucl. Magn. Reson. Spectrosc.* **40**, 175 (2002).
- Dirac, P.A.M., *The Principles of Quantum Mechanics*, Oxford University Press, New York (1967).
- Doddrell, D.M., D.T. Pegg, and M.R. Bendall, *J. Magn. Reson.* **48**, 323 (1982).
- Fano, U., *Rev. Mod. Phys.* **29**, 74 (1957).
- Friebolin, H., *Basic One- and Two-Dimensional NMR Spectroscopy*, 2nd edn, VCH Publishers, New York (1993).
- Harris, J. and H. Stocker, *Handbook of Mathematics and Computational Science*, Springer-Verlag, New York (1998).
- Harris, R.K., E.D. Becker, S.M.C. De Menezes, R. Goodfellow, and P. Granger, *Pure Appl. Chem.* **73**, 1795 (2001).
- Hore, P.J., J.A. Jones, and S. Wimperis, *NMR: The Toolkit*, Oxford University Press, Oxford (2001).
- Howarth, M.A., L.Y. Lian, G.E. Hawkes, and K.D. Sales, *J. Magn. Reson.* **68**, 433 (1986).
- Karplus, M., *J. Am. Chem. Soc.* **85**, 2870 (1963).
- Karplus, M., *J. Phys. Chem.* **30**, 11 (1959).
- Lazzeretti, P., *Prog. Nucl. Magn. Reson. Spectrosc.* **36**, 1 (2000).
- Lipstitz, R.S. and N. Tjandra, *Annu. Rev. Biophys. Biomol. Struct.* **33**, 387 (2004).
- Markley, J.L., A. Bax, Y. Arata, C. W. Hilbers, R. Kaptein, B. D. Sykes *et al.* *J. Biomol. NMR* **12**, 1 (1998).
- Mazzeo, A.R., M.A. Delsuc, A. Kumar, and G.C. Levy, *J. Magn. Reson.* **81**, 512 (1989).
- Morris, G.A. and R. Freeman, *J. Am. Chem. Soc.* **101** 760 (1979).
- Moskau, D., *Concepts Magn. Reson.* **15**, 164 (2001).
- Neuhaus, D. and M.P. Williamson, *The Nuclear Overhauser Effect in Structural and Conformational Analysis*, VCH Publishers, New York (1989).
- Prestegard, J. H., H. M. Al-Hashimi, and J. R. Tolman, *Quart. Rev. Biophys.* **33**, 371 (2000).
- Sibisi, S., J. Skilling, R.G. Brereton, E.D. Laue, and J. Staunton, *Nature (London)*, **311**, 446 (1984).
- Solomon, I. *Phys. Rev.* **99**, 559 (1955).
- Sørensen, O.W., G.W. Eich, M.H. Levitt, G. Bodenhausen, and R.R. Ernst, *Prog. Nucl. Magn. Reson. Spectrosc.* **16**, 163 (1983).
- Spera, S. and A. Bax, *J. Am. Chem. Soc.* **113**, 5490 (1991).
- Stern, A.S. and J.C. Hoch, *J. Magn. Reson.* **97**, 255 (1992).
- Tjandra, N., *Structure* **7**, R205 (1999).
- Tjandra, T. and A. Bax, *Science* **278**, 1111 (1997).
- Wang, A.C. and A. Bax, *J. Am. Chem. Soc.* **118**, 2483 (1996).
- Winder, S., *Analog and Digital Filter Design*, 2nd edn, Elsevier Science (USA) (1997).
- Wishart, D.S., C.G. Bigam, J. Yao, F. Abildgaard, H.J. Dyson, E. Oldfield *et al.* *J. Biomol. NMR.* **6**, 135 (1995).
- Wishart, D.S., F.M. Richards, and B.D. Sykes, *J. Mol. Biol.* **222**, 311 (1991).
- Wüthrich, K., *NMR of Proteins and Nucleic Acids*, John Wiley & Sons, New York (1986).
- Zhu, G. and A. Bax, *J. Magn. Reson.* **90**, 405 (1990).
- Ziessow, D., *Concept Magn. Reson.* **2**, 81 (1990).